CONTINUOUS GREEN DIESEL PRODUCTION VIA HYDROTREATING
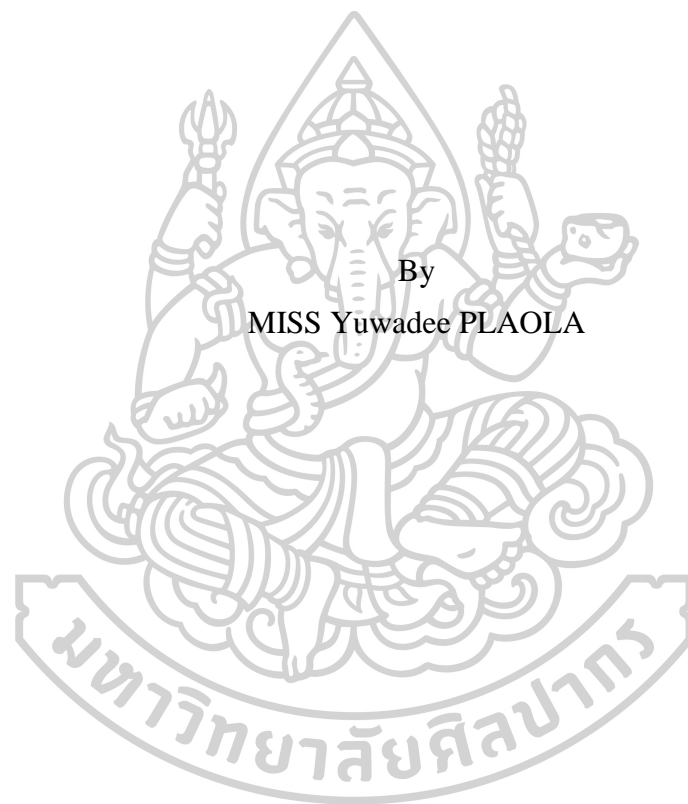UNDER SYNTHESIS GAS ATMOSPHERE

By
MISS Yuwadee PLAOLA

A Thesis Submitted in Partial Fulfillment of the Requirements
for Master of Engineering (CHEMICAL ENGINEERING)
Department of CHEMICAL ENGINEERING
Graduate School, Silpakorn University
Academic Year 2020
Copyright of Graduate School, Silpakorn University

การผลิตกรีนดีเซลแบบต่อเนื่องผ่านกระบวนการไฮโดรทรีตติงภายใต้บรรยากาศแก๊สสังเคราะห์

โดย
นางสาวยุวดี เปลาเล

วิทยานิพนธ์นี้เป็นส่วนหนึ่งของการศึกษาตามหลักสูตรวิศวกรรมศาสตรมหาบัณฑิต
สาขาวิชาวิศวกรรมเคมี แผน ก แบบ ก 2 ระดับปริญญามหาบัณฑิต
ภาควิชาวิศวกรรมเคมี
บัณฑิตวิทยาลัย มหาวิทยาลัยศิลปากร
ปีการศึกษา 2563
ลิขสิทธิ์ของบัณฑิตวิทยาลัย มหาวิทยาลัยศิลปากร

CONTINUOUS GREEN DIESEL PRODUCTION VIA HYDROTREATING UNDER SYNTHESIS GAS ATMOSPHERE

By

MISS Yuwadee PLAOLA

A Thesis Submitted in Partial Fulfillment of the Requirements
for Master of Engineering (CHEMICAL ENGINEERING)
Department of CHEMICAL ENGINEERING
Graduate School, Silpakorn University
Academic Year 2020
Copyright of Graduate School, Silpakorn University

Title   Continuous green diesel production via hydrotreating under synthesis gas atmosphere
By   Yuwadee PLAOLA
Field of Study   (CHEMICAL ENGINEERING)
Advisor   Assistant Professor WORAPON KIATKITIPONG , D.Eng.

Graduate School Silpakorn University in Partial Fulfillment of the Requirements for the Master of Engineering

Dean of graduate school
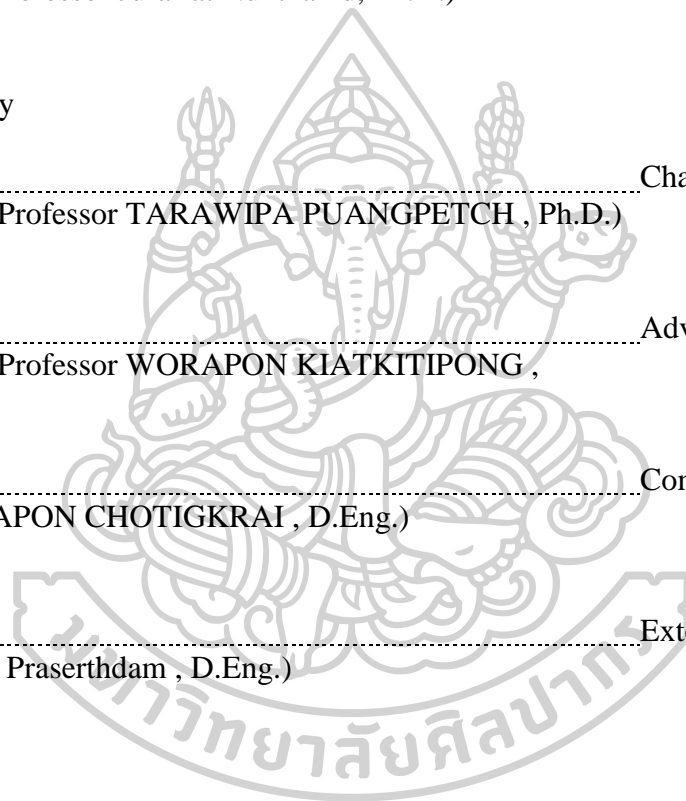(Associate Professor Jurairat Nunthanid, Ph.D.)

Approved by

Chair person
(Assistant Professor TARAWIPA PUANGPETCH , Ph.D.)

Advisor
(Assistant Professor WORAPON KIATKITIPONG , D.Eng.)

Committee
(NUTCHAPON CHOTIGKRAI , D.Eng.)

External Examiner
(Supareak Praserthdam , D.Eng.)

61404205 : Major (CHEMICAL ENGINEERING)
Keyword : sulfided NiMo, NiCu/HZSM-5, Green diesel, Biofuel, Hydrotreating, Synthesis gas, reduced NiMo

MISS YUWADEE PLAOLA : CONTINUOUS GREEN DIESEL PRODUCTION VIA HYDROTREATING UNDER SYNTHESIS GAS ATMOSPHERE THESIS ADVISOR : ASSISTANT PROFESSOR WORAPON KIATKITIPONG, D.Eng.

In this research work, deoxygenation of palm fatty acid distillate (PFAD), an inedible by-product from the palm oil refining process, was investigated over sulfided NiMo/γ-Al$_2$O$_3$ catalyst under synthesis gas as a cheaper alternative to pure hydrogen for lower-cost green diesel production. The experiments were performed in a continuous fixed-bed reactor at 330 °C, operating pressure of 30-50 bar, liquid hourly space velocity = 1 h^{-1}, and gas/feedstock ratio = 250-1000 v/v. Although complete PFAD conversion can be obtained under most studied operating conditions, the higher operating pressure and gas/feed ratio lead to higher diesel yield on both hydrogen and synthesis gas. Under operating pressure of 50 bar with gas/feed ratio of 500 (v/v), synthesis gas offers stable diesel yield approximately 80% during time on stream of 42 h which is not different from using pure hydrogen. For the reaction pathway, as expected, hydrodeoxygenation was found as a dominant reaction pathway for sulfided NiMo/γ-Al$_2$O$_3$ catalyst which the main components were n-C$_{16}$ and n-C$_{18}$ that have the same carbon atom (C$_n$) corresponding to PFAD feedstock. Interestingly, operating under pure synthesis gas promotes higher C$_n$/C$_{n-1}$ than that of pure hydrogen because the carbon monoxide in the synthesis gas acts as a reducing agent to produce C$_n$. Moreover, this research compared edible oil such as palm oil but the result not different. To emphasize the role of carbon monoxide, the deoxygenation reaction was performed under pure carbon monoxide. Carbon monoxide not only increased C$_n$/C$_{n-1}$ ratio but also pronounced isomerization and unsaturated hydrocarbon (alkene) formation. However, when operating under pure carbon monoxide, the PFAD conversion of only 85% can be obtained and dramatically dropped to 50% within 24 h. This could be mainly due to carbon formation. As indicated by thermogravimetric analysis of spent catalysts, carbon formation by operating under pure carbon monoxide is much higher than operating under synthesis gas and pure hydrogen. According to a success of using synthesis gas instead of pure hydrogen with sulfided NiMo/γ-Al$_2$O$_3$ catalyst, preliminary test on other catalysts including reduced NiMo/γ-Al$_2$O$_3$ (as non-sulfided catalyst) and NiCu/HZSM-5 (as cracking catalyst) were performed. The results showed acceptable stability of these catalysts under synthesis gas for at least 42 h of time on stream.

ACKNOWLEDGEMENTS

TABLE OF CONTENTS

Page

LIST OF TABLES

LIST OF FIGURES

Page

CHAPTER I

INTRODUCTION

1.1 Motivation

The global warming problem is a phenomenon in which the earth's temperature rises. The leading cause is the burning of fossil fuels such as coal, oil, and natural gas to produce energy. The gas produced from the burning of fossil fuel or petroleum fuel called greenhouse gases could prevent the earth from reflecting light from the sun. The greenhouse gases, such as CO_2 produced from industrial and transportation sectors. For the transportation sector, biofuel has long been of interest to replace fossil fuel by carbon neutral cycle concepts. Molecules of vegetable oil containing triglyceride and fatty acid are promising to produce alkane hydrocarbon.

The first generation of biodiesel is produced from triglycerides and fatty acids with alcohol via transesterification process. This biodiesel production is performed under mild conditions, which produced fatty acid methyl ester (FAME) as a product and glycerol as a by-product. The biodiesel products from this process have high oxygen content at –COO- ester bonds, thus causing low thermal and oxidation stability [1]. The other disadvantage of FAME is high viscosity and low heating value than petroleum fuel.

The second generation is a catalytic deoxygenation process for green diesel production (also known as "bio-hydrogenated diesel (BHD)"). The green diesel structure is alkane which similar to that of petroleum diesel [2]. The green diesel property was better than FAME, such as high cetane number, zero oxygen containing [3, 4].

There are two main steps of reaction in hydroprocessing. The first step is hydrogenolysis of triglyceride to produce propane and fatty acid. The second step is catalytic deoxygenation to convert fatty acid to a hydrocarbon via three possible reaction pathways, including decarbonylation (DCO), decarboxylation (DCO_2), and hydrodeoxygenation (HDO) reaction. In the hydrogenation derived renewable diesel, the hydrogen and utilities make up approximately 13% (Neste Oil, 2011). The alternative research to reduce the use of hydrogen gas by using inert gas to convert

fatty acid to hydrocarbon via decarboxylation reaction pathway [5-8]. However, pure hydrogen was important for this process in terms of catalyst stability, conversion, and product selectivity. Hydrogen gas is currently produced from the steam reforming of methane. Carbon monoxide in synthesis gas would be converted to hydrogen by water gas shift (WGS) reaction and then further purification process such as pressure swing adsorption is needed. [9-11]. Pongsiriyakul et al [12] originally demonstrated that synthesis gas (a mixture of 70%H_2 and 30%CO) could be used instead of pure hydrogen effectively for green diesel production. Besides, they used palm fatty acid distillate (PFAD), a non-edible by-product from the refine palm oil process, as a feedstock in their study. PFAD consists of high fatty acid about 95wt.% [12] and has a lower cost than refined palm oil.

This research aim to produce green diesel from palm fatty acid distillate (PFAD) over sulfided NiMo/γ-Al$_2$O$_3$ and NiCu/ZSM-5 catalysts under synthesis gas atmosphere in continuous operation.

1.2 Objective of the research

To produce green diesel via hydrotreating process from palm fatty acid distillate (PFAD) in continuous operation under synthesis gas atmosphere.
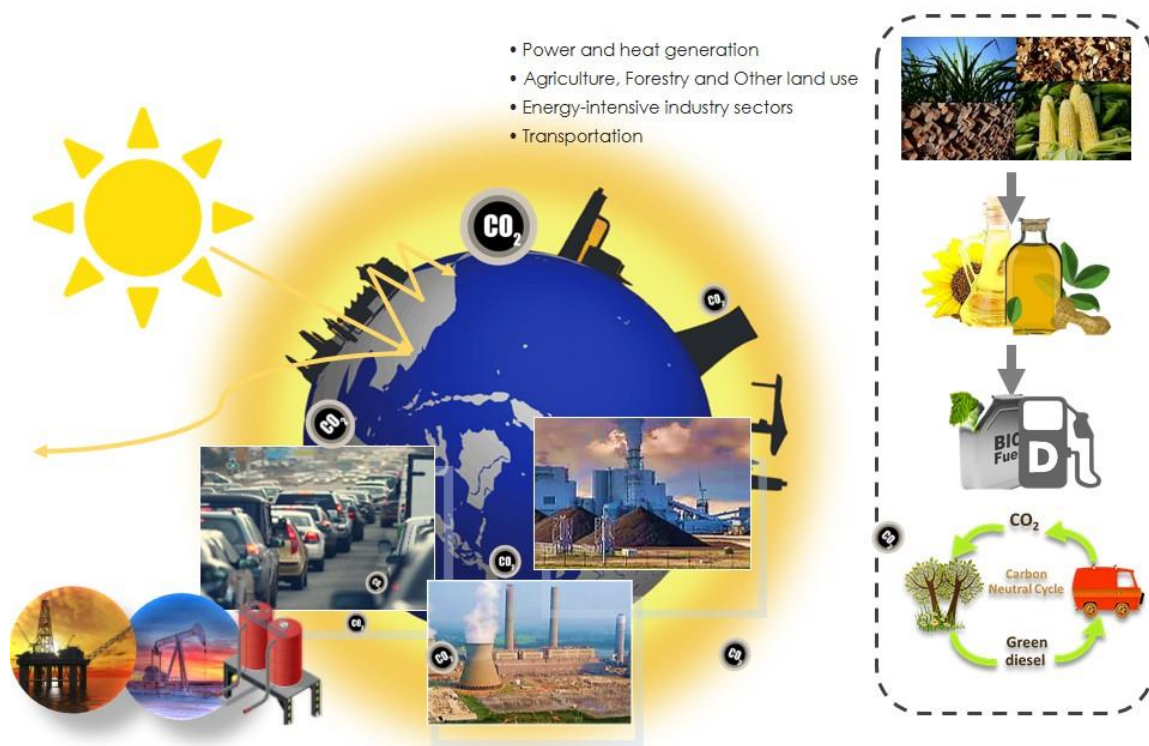
Figure 1 The emission of CO_2 and Carbon neutral cycle.
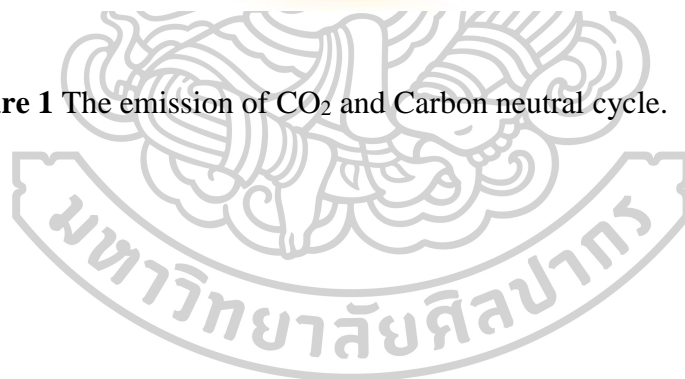
CHAPTER II

LITERATURE REVIEWS

The catalyst used in catalytic deoxygenation affected the reaction pathway and catalyst stability. Many research studies about the type of catalysts to improve this process include sulfide catalysts, metal catalysts, and other forms such as Carbine, Phosphide, Nitride catalyst, etc.

2.1 Sulfided catalyst

David Kubicka., et al. [13] studied the deoxygenation of vegetable oils for biofuel production by Ni, Mo, and NiMo sulfided catalyst supported on alumina (Al_2O_3). This research varied the operating conditions of 260-280 °C, 3.5 MPa, and 0.25-4 h^{-1} in a fixed-bed reactor. The result showed the bimetallic NiMo catalysts yield is higher than monometallic catalysts. The dominant reaction pathways of NiMo catalyst are decarboxylation and hydrodeoxygenation. The transformation of triglyceride into hydrocarbons showed in Figure 2.
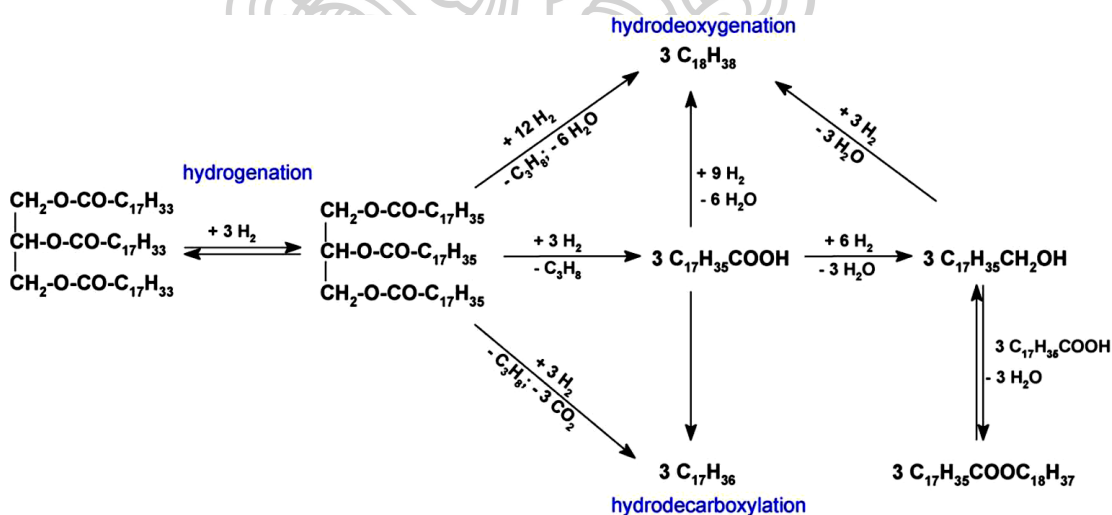
Figure 2 The reaction network for catalytic deoxygenation of vegetable oils to hydrocarbon.

Huber et al. [14] studied the hydrotreating of pure sunflower oil over sulfide $NiMo/Al_2O_3$ at 300-350 °C, 5 MPa H_2, and LHSV of 5.2 h^{-1}. In the first step of this reaction pathway, the triglyceride was hydrogenated and broken down into various intermediates: monoglycerides, diglycerides, and carboxylic acids. These intermediates are then converted into alkanes by three different pathways: decarboxylation, decarbonylation, and hydrodeoxygenation pathway. The hydrocarbon from hydroprocessing process can undergo isomerization and cracking to produce isomerized and lighter alkanes, respectively. As a result, the sunflower oil converted to hydrocarbon via major reaction pathways is decarboxylation and decarbonylation, the primarily n-C_{17} as a primarily liquid product. A carboxylic acid can be converted into methyl group and CO via decarbonylation pathway, while the decarboxylation pathway converts a carboxylic group to an alkane and CO_2 by no consume H_2. The bifunctional catalysis contains NiMo as a site for hydrogenation reactions and dehydration reactions.

Srifah et al. [15] studied to understand the deoxygenation behaviors at different conditions. The bio-hydrogenated catalytic hydrotreating of palm oil over $NiMoS_2/\gamma$-Al_2O_3 catalyst in a continuous fixed-bed reactor to find the optimal hydrotreating conations: 270-420 °C, 15-80 bar, LHSV of 0.25-5.0 h^{-1}, and H_2/oil ratio of 250-2000 N(cm^3 cm^{-3}). The results showed the product yield increase from 26.7% to 89.8% with increasing temperature from 270 to 300 °C. On the other hand, the decrease in product yield from 88.9% to 37.9% with increasing temperature from 330 °C to 420 °C becauseisomerization, cracking, and cyclization reactions are promoted at high temperature. The percent of HDO higher with increasing pressure, while DCO/DCO_2 increasing with decreasing H_2 pressure. The effect of liquid hourly space velocity (LHSV) is used to determine the contact time between feed and catalyst. The increase in LHSV slightly dropped in the product yield. The increased contact time (at low LHSV) would promote the cracking and isomerization reactions. The hydrogen to oil ratio is the ratio of hydrogen feed to the liquid feed, which the parameter is an economic feasibility and hydrotreating processes. The H_2/oil ratio showed a small impact on the conversion. However, dramatically in product yield from 45.2% to 93.3% with the H_2/oil ratio from 250-1500 N(cm^3/cm^3).

Kubicka. et al. [3] studied the effect of supports i.e., SiO_2, TiO_2, and Al_2O_3 with sulfide NiMo catalyst in deoxygenation of rapeseed oil (food grade quality, without the addition of sulfiding agent) in a fixed bed reactor at 3.5 MPa of H_2, 260-300 °C, H_2/oil ratio 50 mol mol^{-1} and WHSV for 2-8 h^{-1}. The activities of catalyst characteristic by triglyceride conversion and percent of deoxygenation. The activity of catalysts decreases in order $SiO_2 > Al_2O_3 > TiO_2$. The high surface area and high dispersion of NiMo/SiO_2 catalyst exhibited a smaller extent of hydrogenation reaction and a larger extent of decarboxylation.

Liu et al. [2] studied the hydrotreatment to produce bio-hydrogenated diesel (BHD) and liquefied petroleum gas (LPG) fuel by one-step hydrotreatment process from different amounts of fatty acids vegetable oils (jatropha oil, palm oil, and canola oil) over NiMo based catalysts in a high-pressure fixed-bed flow reaction system at reaction temperature, 350 °C, H_2 pressure of hydrogen, 40 bar, H_2/oil ratio in feed 800 mL mL^{-1}. NiMo/SiO_2 formed n-$C_{18}H_{38}$, n-$C_{17}H_{36}$, n-$C_{16}H_{34}$, and n-$C_{15}H_{32}$ as predominant products in the hydrotreatment of jatropha oil. Either NiMo/H-Y or NiMo/H-ZSM-5 was not suitable for producing BHD because a large amount of gasoline-ranged hydrocarbons was formed on the strong acid sites of zeolites. The liquid hydrocarbons formed over NiMo/SiO_2 catalyst contained the lowest *iso/n* ratio (0.3), the high pour point (20 °C), while the pour point of liquid hydrocarbon over NiMo/γ-Al_2O_3 catalyst was high (10 °C) in comparison with normal diesel (-15 °C). When SiO_2-Al_2O_3 was used as a support for the Ni-Mo catalyst, the pour point of the liquid hydrocarbon product of -10 °C and *iso/n* ratio of 0.26 by converting some C_{15}-C_{18} n-paraffins to *iso*-paraffins and light paraffin could be obtained. Because SiO_2-Al_2O_3 had a proper solid acidic strength to support NiMo to produce BHD from vegetable oils.

Jozef Mikulec., et al. [16] studied transformation of triacylglycerols to diesel fuels over commercially available NiMo and NiW hydrorefining catalysts. It was proved that during hydrodesulphurisation also hydrodeoxygenation occurs and triacylglycerols can be converted to the fuel biocomponent by adding 6.5% vol. of the triacylglycerols to atmospheric gas oil. In this way, after hydroprocessing at conditions are temperature 320–360 °C, pressure 35–55 bar, LHSV: 1.0 h^{-1} and ratio H_2:HC 500–1000 N(m^3 $m^{-3)}$, catalyst presence), gas oil containing 5–5.5% of

biocomponent was prepared, characterized with performance and emission parameters similar to fossil diesel. The process was tested using NiMo and NiW catalysts on various catalyst supports. The results are interested in NiMo/TiO$_2$ catalyst at condition temperature 360 °C, pressure 35 bar, LHSV 1 h^{-1}, H$_2$:HC+TAG 1000 Nm^3 m^{-3} and feed AGO+RO showed 2.32 of n-C$_{17}$/n-C$_{18}$ and aromatics 26.2 wt.%, while NiMo/TiO$_2$ catalyst at condition temperature 360 °C, pressure 35 bar, LHSV 1 h^{-1}, H$_2$:HC+TAG 1000 Nm^3 m^{-3}, feed AGO+RO, n-C$_{17}$/n-C$_{18}$ 2.32 and aromatics 26.2 wt.%.

Aqsha et al. [17] studied hydrodeoxygenation of bio-oil: guaiacol as a model component among various catalysts, NiMo/TiO$_2$ was chosen to understand the influence of reaction parameters, such as temperature, reaction time, H$_2$ pressure, and quantity of the catalyst. As there is an increase in the temperature (200, 250, 300 and 350 °C), reaction time (1, 5, 8 and 24 h), H$_2$/guaiacol molar feed ratio (0:1, 1:2, 1:1, and 2:1), and catalyst amount (0, 25, 50 and 100 mg), the conversion has increased significantly while maintaining the high selectivity to HDO products without ring opening reactions. Under optimized conditions (350 °C and 2:1 of H$_2$: guaiacol ratio), 98% guaiacol is converted on NiMo/TiO$_2$ resulting phenol, polymethyl substituted phenols and traces of cyclohexanone and benzene. H$_2$/guaiacol ratio NiMo/TiO$_2$. Reaction conditions: 10 wt.% catalyst to guaiacol; 300 °C 5 h. The guaiacol conversion was very low in the absence of hydrogen (< 20%) with catechol dimethyl ether and catechol as the primary products. As H$_2$ pressure increases, the guaiacol conversion is increased significantly from 20 to 67%.

Nimkarde et al. [18] studied hydrotreatment of vegetable oil or green diesel or second-generation biofuel. This study using the non-edible *Pongamia pinnata* oil or Karanja oil at temperature (573-653 K), pressure (1.5-3.5 MPa), and H$_2$/oil ratios (400-600 v/v) over sulfided NiMo and CoMo catalysts supported on γ-Al$_2$O$_3$ in a fixed-bed reactor. The oil conversion increases with increasing pressure for both catalysts. At high pressure facilitates deoxygenation of triglycerides and breaking of the glycerol backbone but high energy cost and decreased the product yield as a result of enhanced formation of lighter products such as propane, methane, and water. , Oil conversion decreased with the rise in space velocity for both catalysts. The Ni-based catalyst exhibited a higher performance than Co-based catalysts.

Thongkumkoon et al. [19] studied the improvement of catalytic activity by trimetallic sulfided Re-Ni-Mo/γ-Al$_2$O$_3$. The loading of Re as a promoter into NiMo catalyst investigated by SEM-EDS of sulfide 3%Ni-10%Mo/γ-Al$_2$O$_3$ and 1%Re3%Ni-10%Mo/γ-Al$_2$O$_3$. The results showed when load Re exhibited a highly dispersed and elemental compositions of Ni and Mo and S over sulfided 3%Ni-10%Mo/γ-Al$_2$O$_3$ were 2.7, 7.8 and 8.1 wt.%, respectively while elemental compositions of Ni and Mo and S over sulfided 1%Re3%Ni-10%Mo/γ-Al$_2$O$_3$ were 3.6, 9.3 and 10.1 wt.%, respectively. It can be concluded that the Re as a promoter to reduce the cluster size of metal sulfide particles and improve the dispersion of metal Ni and Mo species over γ-Al$_2$O$_3$ support. The effect of trimetallic on liquid products and gas products, the Re-Ni-Mo/γ-Al$_2$O$_3$ catalyst could improve the diesel yield from 61.63% to 79.59% and increased C$_{15}$-C$_{17}$ isoparaffins due to the sulfided Re-Ni-Mo/γ-Al$_2$O$_3$ catalyst favored isomerization reaction than sulfided Ni-Mo/γ-Al$_2$O$_3$ catalyst. The increasing of isomerization degree provided a lower cloud point.

Itthibenchapong et al. [20] studied the preparation of NiMoS$_2$ over γ-Al$_2$O$_3$ support by using thiourea (CS(NH$_2$)$_2$) as a sulfur agent for deoxygenation of biofuel to produce renewable jet fuel-like hydrocarbon from palm kernel oil. The experiment was performed in a trickle bed reactor with temperature of 270-330 °C, pressure of 30-50 bar, LHSV of 1-5 h^{-1} and H$_2$/oil ratio of 1000 N(cm^3 cm^{-1}). The result showed side reaction is cracking was favorable at high temperatures. Moreover, the methanation reaction can occur at 300 °C due to CO was decreased. The alkane C$_{10}$-C$_{12}$ in biofuel products improved the cloud point (6.2 °C) and pour point (-3.0 °C) and maintained a high heating value of 46.6 MJ kg^{-1} that suitable for blending with fossil jet or diesel fuel. The isomerization can be improved cold flow property.

Kim et al. [21] studied renewable diesel production via catalytic deoxygenation of triglycerides. This work used refined soybean oil as a triglyceride feedstock in batch operating over Ni, Pd and sulfided CoMo and NiMo catalysts. The reaction for the formation of intermediates and hydrocarbons showed in Figure 3. Broken lines represent bond scission. The proposed chemistries involved in the conversion of aldehydes to ketones are shown schematically in the box. The end-product characteristics corresponding to each catalyst are emphasized by the underlined labels. Firstly, triglyceride was hydrogenated into fatty acid and found the

formation of aldehyde as the first intermediate. Then deoxygenation reaction was started by C-O bond cleavage via the Hydrodeoxygenation pathway, while C-C bond cleavage via Decarboxylation/Decarbonylation pathway. In the case of sulfide catalyst, the isomerization occurred but in the case of a noble metal catalyst cyclization occurred.
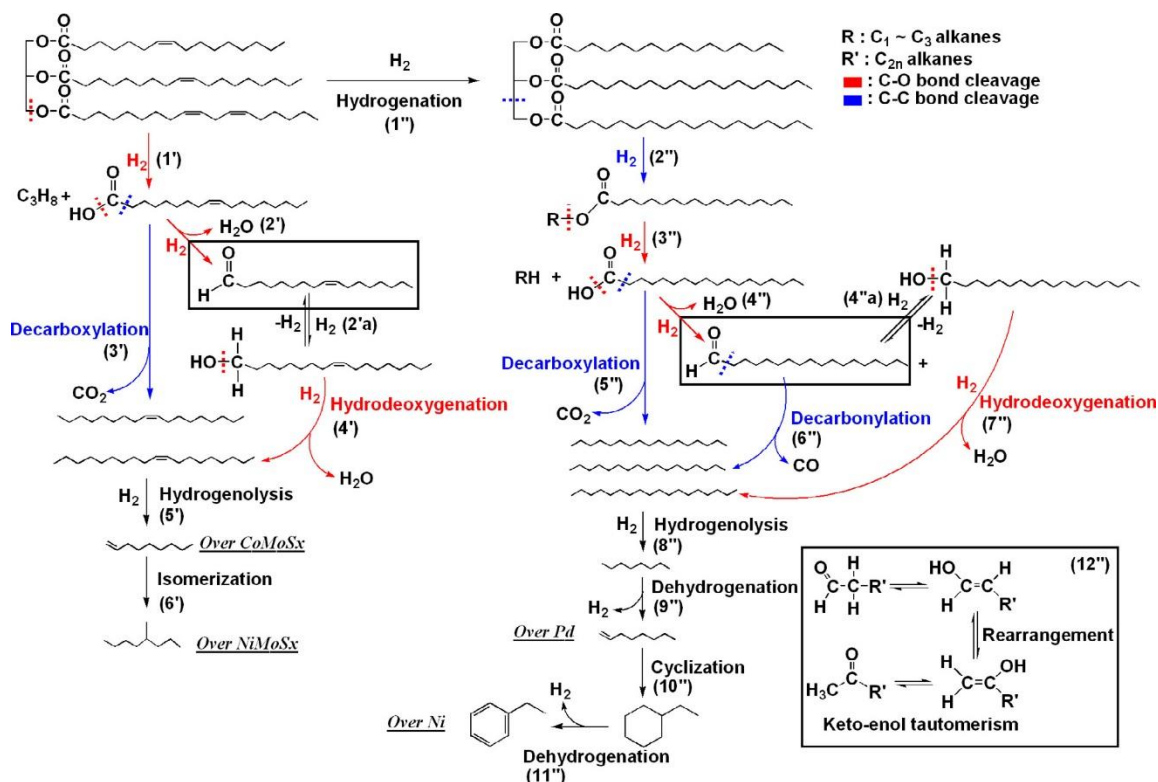
Figure 3 The general reaction pathways of a triglyceride over four types of catalysts [21].

2.2 Metallic catalyst

2.2.1 Noble metal catalyst

Chen et al. [4] studied the ratio of Si/Al on the noble metal Pt/SAPO-11 catalyst with Jatropha oil as a feedstock. The result indicated that 3 wt% Pt is the best Pt loading on SAPO-11 support catalyst, which generated an 83 % yield of iso-C_{15}-C_{18} hydrocarbons. The n-alkanes from triglycerides molecule diffused into the ordered micropores of SAPO-11 for isomerization or cracking. Therefore, when the Pt loading was increased, the isomerization and cracking activities.

Ala'a H., et al. [22] studied the synthesis of active catalysts from waste date pits carbon produced by carbonization and impregnation with Pt and Pd metals that high surface area. The result indicated the hydrodeoxygenation reaction to jet fuel and green diesel fraction production. The results indicated that the degree of deoxygenation (DOD) of product oil was 97.5% and 89.4% for the Pd/C and Pt/C catalysts, respectively. The main products are paraffinic hydrocarbons. The maximum fraction of hydrocarbons of 72.03% and 72.78% green diesel were obtained by using Pd/C and Pt/C catalysts, respectively.

Sotelo-Boyas R., et al. [23] studied catalytic hydrotreating of rapeseed oil over NiMo/γ-Al_2O_3, Pt/H-Y and Pt/H-ZSM-5 catalyst in a batch reactor over 300-400 °C and H_2 and pressure of 5-11 MPa. The results showed the sulfide NiMo/γ-Al_2O_3 gave the highest yield of a diesel-like hydrocarbon containing mainly n-paraffins (n-C_{15}- n-C_{18}) about 70-80% while the yield of isoparaffins is very low. The gas product mainly carbon dioxide that decarboxylation as major reaction pathway because the batch reactor, the hydrogen pressure continuously decreasing and possible reaction can occur in the process from carbon monoxide and water are transformed into carbon dioxide and hydrogen. Besides, carbon monoxide could be steam-reformed to generate hydrogen that advantage to produce green diesel. The liquid hydrocarbon in diesel range from NiMo/γ-Al_2O_3 catalyst has a high cetane number and high pour point. This work-study using Pt/Zeolite catalyst to improve cold properties by transforming these n-paraffins into iso-paraffins, which have a very low pour point because the isomerization reaction is promoted by the acid sites of the catalyst. Both Pt/Zeolite produced gasoline yield (C_5-C_{12}) very low about 20-40% and a high

concentration of *iso*-paraffins with better cold flow properties than NiMo/γ-Al$_2$O$_3$ catalyst.

Veriansyah et al. [24] studied the effect of catalysts on the hydroprocessing process to produce renewable diesel by using soybean oil as a feedstock under 400 °C, reaction time of 2 h. The order hydroprocessing conversion was NiMo/γ-Al$_2$O$_3$ (92.9%) > Pd/γ-Al$_2$O$_3$ (91.9%) > CoMo/γ-Al$_2$O$_3$ (78.9%) > Ni/SiO$_2$-/γ-Al$_2$O$_3$ (60.8%) > Pt/γ-Al$_2$O$_3$ (50.8%) > Ru/γ-Al$_2$O$_3$ (39.7%). The Pt catalyst promoted hydrogenation when compared to the other catalysts but low conversion of hydroprocessing. The larger amount of propane gas in the gas product indicates that a more active hydrocracking reaction occurred with the Pt catalyst. The n-alkane of liquid product from Pd or Ni catalyst was more than 80 wt.%. In comparison, it was less than 55 wt.% for the CoMo catalyst and higher naphtha selectivity suggested that isomerization and cracking reaction. The use of Ni, NiMo, and CoMo are low-cost catalysts suitable for use in the hydroprocessing. The noble metal catalysts have exhibited desirable deoxygenation activity to yield high amounts of hydrocarbons. However, the noble metal catalyst high-cost therefore, many work-study non-noble metal catalysts.

2.2.2 Non-noble metal catalysts

Kaewmeesri et al. [25] studied green diesel production using waste chicken fat as a feedstock contains a high degree of free fatty acids (FFAs) and water over a Ni/γ-Al$_2$O$_3$ catalyst in a trickle-bed reactor. The condition of hydroprocessing is performed at a temperature of 330 °C, H$_2$ pressure of 50 bar, LHSV of 2.0 h^{-1}, and H$_2$/oil ratio of 1000 (cm^3 cm^{-3}). In both cases of the effect of water content and fatty acid in the waste chicken fat feedstock, the result showed water content (4 wt.%) and a high degree of fatty acids in can improve the bio-hydrogenated yield and promote DCO/DCO$_2$ as major reaction pathway which required less H$_2$ consumption.

Srifah et al. [17] studied the green diesel production via the hydrodeoxygenation of palm olein using γ-Al$_2$O$_3$-supported monometallic catalysts (Co, Ni, Pd, and Pt) in a continuous fixed-bed reactor under the conations 270-420 °C, 15-80 bar H$_2$, LHSV of 0.25-5.0 h^{-1}, and H$_2$/oil ratio of 250-2000 N(cm^3/cm^3). The result showed that the deoxygenation activity decreased in the order of product

yield Co > Pd > Pt > Ni. The conversion over pure γ-Al_2O_3 about 56% without diesel product yield. They suggest that only saturated triglyceride scission to fatty acids and propane occurred. The reaction pathway of Ni, Pd, and Pt catalysts (Figure 4) were favorable to the DCO route, whereas DCO/DCO_2 and HDO were all dominant over the Co catalyst. The decarbonylation reaction was more dominant than the hydrodeoxygenation reaction when the reaction was catalyzed by Ni, Pd, and Pt catalysts. Meanwhile, the contribution of decarbonylation and/or decarboxylation was nearly comparable to that of the hydrodeoxygenation reaction over Co catalyst.
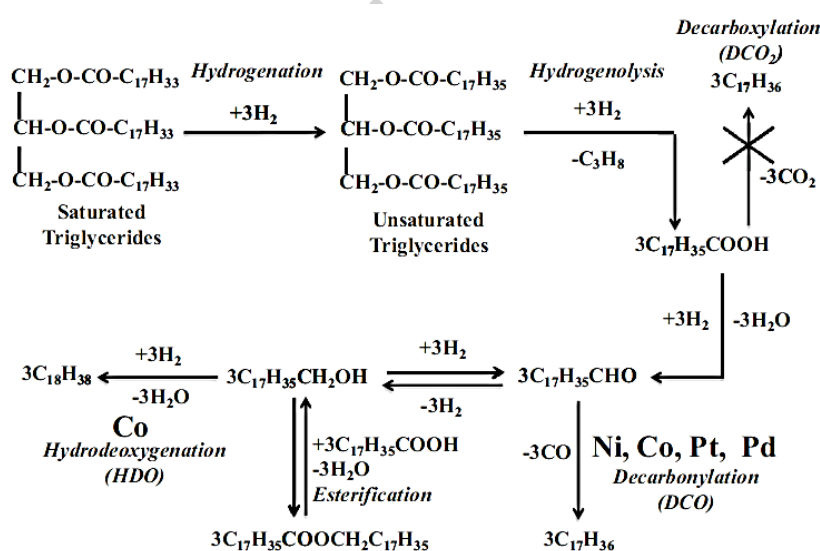
Figure 4 The reaction pathway of Ni, Co, Pd, and Pt catalysts.

Wirikulcharoen et al. [26] studied bio-jet fuel production via continuously hydrotreating process by using palm oil (palm refined olein) as a feedstock over cracking NiCu/HZSM-5 catalyst. The operating condition at 400 °C, 40 bar of H_2, LHSV of 2 h^{-1}, and H_2/oil ratio of 1000 N(cm^3 cm^{-3}). Initially, palm oil conversion stable to 36 h and dramatically decreased from 90% to 37% over 80 h to 103 h. It caused by coke deposition on the catalyst's surface.

The deactivation of reduced Ni/γ-Al$_2$O$_3$ and Co/γ-Al$_2$O$_3$ catalysts in hydrodeoxygenation of palm oil in a continuous trickle bed reactor under the conations 300 °C, 5 MPa H$_2$, LHSV of 1 h^{-1}, and H$_2$/oil ratio of 1000 N(cm^3 cm^{-3}). The major reason for catalyst deactivation from the results of catalyst characterization by XRD, TEM and TPO analyses revealed some sintering of the nickel and cobalt particles during the time course of the reaction. In TPO analysis, the carbon deposition rate on the cobalt catalyst was faster than that on the nickel catalyst [27].

2.3 Carbine, Phosphide, and Nitride catalyst

Monnier et al. [28] studied hydrodeoxygenation of oleic acid as a feedstock using nitrides of molybdenum, tungsten, and vanadium over the γ-Al$_2$O$_3$ catalyst. The gas product concentration of CO and CO$_2$ as compared with water gas shift equilibrium at 380 °C, 8.3 MPa H$_2$, the calculation showed the actual outlet concentrations of gas products are very closed to the WGS thermodynamic equilibrium for molybdenum and tungsten catalysts. The authors indicated that molybdenum and tungsten are good WGS catalysts. The liquid products from nitrides of vanadium and tungsten are promoted by the decarboxylation and decarbonylation reaction pathways, while the nitrides of molybdenum favor the hydrodeoxygenation as a reaction pathway.

Wang, F., et al. [29] studied the use of Mo$_2$C and W$_2$C supported on activated carbon catalysts to produce green diesel from fatty acids in a batch reactor. In the proposed pathway, the unsaturated fatty acids convert into saturated fatty acids and the saturated fatty acids are converted into C$_{17}$ or C$_{15}$ alkanes. The conversion of fatty acids over the Mo$_2$C/AC catalyst was remarkably higher than W$_2$C/AC because the particle of molybdenum compounds was finer and dispersed more than tungsten compounds. The main reaction pathway of both catalysts is hydrodeoxygenation.

Various oil sources, reactor type, reaction conditions, supported metal sulfide catalysts, main products obtained during hydrotreating of vegetable oil are summarized in Table 1.

Table 1 The catalyst and condition of bio-hydrogenated diesel reaction in continuous operation.

Catalyst	Feedstock	Condition	Performance	Ref.
Metal catalysts				
-non noble catalysts				
NiMoCe (5wt%)/γ-Al$_2$O$_3$	Jatropha oil	370 °C, 35 bar of H$_2$, LHSV= 0.9 h^{-1} H$_2$/oil = 1000 (v/v)	Conversion = 89% yield of C$_{15}$-C$_{18}$ = 80%	[30]
Co(5wt%)/ γ-Al$_2$O$_3$	Palm oil	330 °C, 50 bar of H$_2$, LHSV= 2 h^{-1} H$_2$/oil = 1000 (v/v)	Conversion = 100% yield of C$_{15}$-C$_{18}$ = 94.3%	[17]
CoMo/γ-Al$_2$O$_3$	Sunflower oil	380 °C, 40 bar of H$_2$, LHSV= 1 h^{-1} H$_2$/oil = 1000 (v/v)	Conversion = 100% yield of C$_{15}$-C$_{18}$ = 83%	[31]
NiMo-S/γ-Al$_2$O$_3$	Canola oil	325 °C, 31 bar of H$_2$, LHSV= 1 h^{-1} H$_2$/oil = 600 (v/v)	Conversion = 98% yield of C$_{15}$-C$_{18}$ = 73.9%	[32]
Sulfided CoMo/γ-Al$_2$O$_3$	Jatropha oil	380 °C, 30 bar of H$_2$, LHSV= 2 h^{-1} H$_2$/oil = 4.5 (v/v)	Conversion = 97% yield of C$_{15}$-C$_{18}$ = 62.6%	[33]
Sulfided NiMo/γ-Al$_2$O$_3$	Karanja oil	380 °C, 30 bar of H$_2$, WHSV= 5 h^{-1} H$_2$/oil = 600 (v/v)	Conversion = 88% yield of C$_{15}$-C$_{18}$ = 75%	[18]
Sulfided NiMo/γ-Al$_2$O$_3$	Rapeseed oil	260-280 °C, 35 bar of H$_2$, LHSV= 0.25-4 h^{-1} H$_2$/oil =1200 (v/v)	Conversion = 30-100%	[13]
Sulfided NiMo/Al$_2$O$_3$-SiO$_2$	Jatropha oil	350 °C, 30 bar of H$_2$, LHSV= 2 h^{-1} H$_2$/oil =600 (v/v)	yield of C$_{15}$-C$_{18}$ = 88.2 %	[34]

Sulfided NiMo/ZHM-5-Al$_2$O$_3$	Jatropha oil	350 °C, 30 bar of H$_2$, LHSV= 2 h^{-1} H$_2$/oil =600 (v/v)	yield of C$_{15}$-C$_{18}$ = 40.34 %	[34]
Sulfided NiMo/γ-Al$_2$O$_3$	Waste cooking oil	350-390 °C, 13.7 bar of H$_2$, LHSV= 0.5-2.5 h^{-1} H$_2$/oil =1068 (v/v)	yield of C$_{15}$-C$_{18}$ =73.7-73.9%	[33]
Sulfided NiMo/γ-Al$_2$O$_3$-F	Sunflower oil	350-370 °C, 20-40 bar of H$_2$, LHSV= 1 h^{-1} H$_2$/oil =500 (v/v)	yield of C$_{15}$-C$_{18}$ =73.2-75.6 %	[35]
NiMoS$_2$/γ-Al$_2$O$_3$	Palm oil	330 °C, 50 bar of H$_2$, LHSV= 1 h^{-1} H$_2$/oil = 1000 (v/v)	Conversion = 100% yield of C$_{15}$-C$_{18}$ = 88%	[15]
Sulfided NiMo/γ-Al$_2$O$_3$	Rubber seed oil	350 °C, 35 bar of H$_2$, LHSV= 1 h^{-1} H$_2$/oil = 1000 (v/v)	Conversion = 99% yield of C$_{15}$-C$_{18}$ = 84.87%	[36]
-noble catalysts				
Pt (1.41wt%) /SAPO-11(0.4)	Jatropha oil	350 °C, 30 bar of H$_2$, LHSV= 1 h^{-1} H$_2$/oil =1200 (v/v)	Conversion = 100% yield of C$_{15}$-C$_{18}$ = 82.8%	[4]
Other catalysts				
Mo$_2$C/REO	Oleic acid	350 °C, 50 bar of H$_2$, LHSV= 2 h^{-1} H$_2$/oil = 4.5 (v/v)	Conversion = 95% yield of C$_{15}$-C$_{18}$ = 85%	[37]
Mo$_2$N/γ-Al$_2$O$_3$	Canola oil	350-370 °C, 20-40 bar of H$_2$, LHSV= 1 h^{-1} H$_2$/oil =500 (v/v)	yield of C$_{15}$-C$_{18}$ =73.2-75.6 %	[28]

Kim, et al. [16] studied the effect of fatty acid compositions of triglyceride on catalytic deoxygenation activity. The increased unsaturated fatty acid of the triglycerides caused heavy products. These heavy products were transformed into coke species and caused catalyst deactivation.

Tanneru et al. [11] studied the catalytic deoxygenation of pretreated bio-oil to produce liquid hydrocarbon performed in a batch autoclave reactor. This research considered an expensive hydrogen problem. The general HDO reaction and the hydrogen can be produced from the water gas shift reaction shown in Figure 5.

$$\text{Catalyst}$$
$$-(CHO)- + H_2 \rightarrow -(CH)- + H_2O$$

$$\text{Catalyst}$$
$$CO + H_2O \leftrightarrow H_2 + CO_2$$
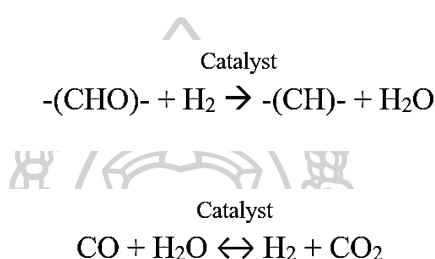
Figure 5 The general HDO and the water gas shift reaction pathways.

First the pretreatment of bio-oil by oxidation reaction converts aldehydes into carboxylic acids. The catalytic deoxygenation consists of 1st-stage partial deoxygenation and 2nd-stage full deoxygenation. The 1st-stage operates at a temperature of 360 °C and under pressurized syngas by a mixture of nickel on silica-alumina (5 wt.%), potassium carbonate (3 wt.%) and copper (II) oxide (2 wt.%) catalyst at 5.5 MPa for 90 min. The syngas was used in studies consist of 18% hydrogen, 22% carbon monoxide, 11% carbon dioxide, 2% methane and 47% nitrogen. The partially deoxygenated product or boiler fuel had an aqueous fraction at the bottom of the vessel and oil phase at the top. The organic fraction was deoxygenated by fully deoxygenated hydrogen. In the 2nd-stage, the fully deoxygenated by a mixture of nickel on silica-alumina (5 wt.%) and copper (II) oxide (2 wt.%) catalyst at a temperature of 425 °C and under pressurized hydrogen at 9.6 MPa for about 150 min. The properties of an oxidized product, boiler fuel and hydrocarbon mixture were analyzed by high heating value, acid value, water content, pH, density, and viscosity. The properties of the boiler fuel and hydrocarbon mixture were improved about the oxygen content, acid value and water content decreased, while higher heating value increased. The gas product mainly CO_2 from the syngas

partial deoxygenation reaction by high consumption of CO that corresponding to the WGS reaction occurred between the CO and H_2O present in the bio-oil. The hydrogen consumption of syngas partial deoxygenation reaction was reduced by approximately 66% compared to the full deoxygenation reaction.

K. Pongsiriyakul., et al. [12] studied hydrocarbon biofuel production via hydrotreating under synthesis gas instead of pure hydrogen. Synthesis gas as a deoxygenating agent in hydroprocessing of PFAD (palm fatty acid distillate) was used as a low-cost feedstock from the refining palm oil process and Pd/C as a catalyst. The hydrotreating was performed in a batch reactor at 40 bar of syngas (consists 70% H_2 and 30% CO) and temperature of 370-400 °C. The liquid product's main components at all operating conditions of both synthesis gas and pure hydrogen were n-C_{15} and n-C_{17}. The reaction pathways for deoxygenation of palmitic acid were shown in Figure 6. The palmitic acid is hydrogenated to intermediate as aldehyde and undergoes a decarbonylation reaction as a major reaction pathway. The main components in the liquid products at all operating conditions of both synthesis gas and pure hydrogen were n-C_{15} and n-C_{17}, in which a slightly lower BHD yield under synthesis gas. CO in the syngas can act as a reducing agent, removing oxygen atoms from fatty acid to form alkenol that could be further reduced to alkene and then cyclized to cycloparaffins.
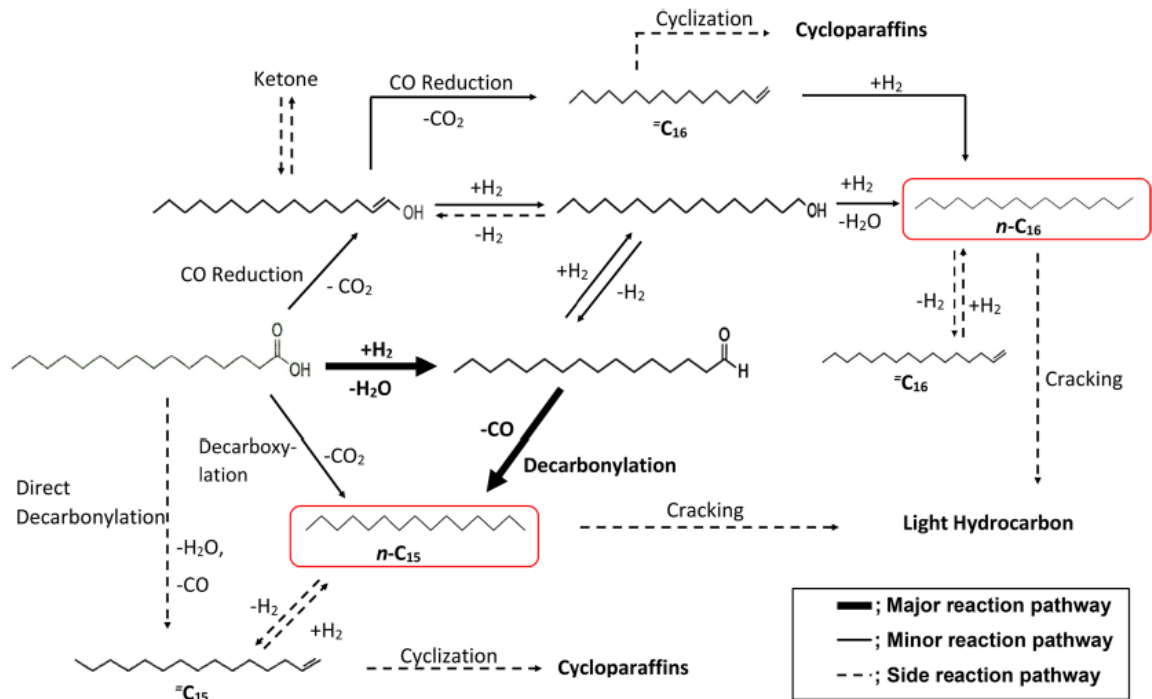
Figure 6 The reaction pathway for hydrotreating process via carbon monoxide.
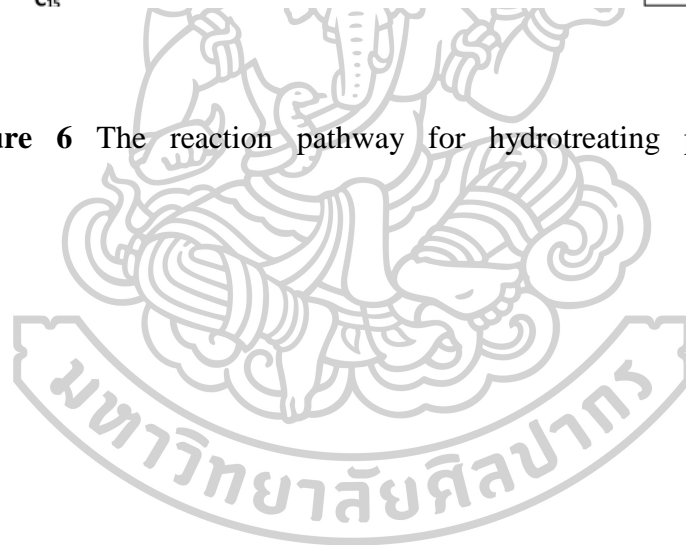
CHAPTER III

THEORY

3.1 Green diesel fuel

The purpose of green diesel production (as called bio-hydrogenated diesel, BHD) is to reduce the use of petroleum fuel because The physicochemical properties of BHD are similar to conventional diesel as shown in Table 2. The higher viscosity of the fuel may cause operational problems in the diesel engine results in poor atomization of fuel and droplet formation. The calorific value defines the quality of heat on complete combustion. Cetane number of green diesel and biodiesel suitable for diesel engines.

Table 2 The physicochemical properties of diesel, biodiesel and BHD [38].

Parameter	EURO-IV Diesel specifications	Karanja biodiesel	BHD (Green diesel)
Density (kg m^{-3})	820-845	881	780
Kinematic Viscosity at 40 °C (mm^2 s^{-1})	2.0-4.5	4.41	2.5-3.5
Flash point (°C)	35-66	168	120-138
Pour point (°C)	3.0-15.0	5	9
Could point (°C)	-	12	-5 to -30
Calorific value (MJ kg^{-1})	-	37.98	44
Cetane number	51	50.8	80-90
Acid value (mg KOH g^{-1})	-	0.43	33.3
S (mg kg^{-1})	50	20	< detect limit
O (wt.%)	-	12.8	0
Distillation (°C)	-	394	265.320
Lubricity (µm)	460	-	360

3.2 Hydroprocessing Process

The triglyceride can be converted into *n*-paraffin and *iso*-paraffins by catalyst under high hydrogen pressure and high temperature. First, the triglyceride molecule cracked to fatty acid and propane by reacted with hydrogen gas. A catalytic reaction of triglycerides through three major reaction pathways was shown in Figure 7, including decarbonylation (DCO), decarboxylation (DCO_2) and hydrodeoxygenation (HDO) reaction pathways. The other possible reaction that occur in hydroprocessing process is gas-phase reaction i.e. reverse water gas shift and methanation reaction [24, 39, 40]. The thermodynamic data of deoxygenation reaction was shown in Table 3.

3.2.1 Decarbonylation reaction

The product from decarbonylation endothermic reaction is Carbon monoxide gas and water by using hydrogen and the alkane or alkene that have carbon atom shorter than the amount of carbon atom in the fatty acid molecule.

3.2.1 Decarboxylation reaction

This reaction's advantage is not consumed hydrogen in the reaction and the carbon atom in the fatty acid molecule was released to produce carbon dioxide.

3.2.3 Hydrodeoxygenation reaction

The hydrodeoxygenation is an exothermic reaction, so at high temperature this pathway as a dominant reaction pathway. In this reaction, the amount of carbon atom in fatty acid and the liquid product is the same. However, hydrogen consumption was higher than decarbonylation and decarboxylation. The by-products from this reaction pathway is water.

3.2.4 Revers water-gas shift and methanation reaction

The gas products are CO_2, CO and H_2 can occur i.e. reverse water-gas shift and methanation reaction.

Table 3 The thermodynamic data for deoxygenation reaction and other reactions [40, 41].

Liquid-phase reaction	Equation	$\Delta G°_{533}$ [kJ mol^{-1}]	$\Delta H°_{533}$ [kJ mol^{-1}]
HDO:	$RCOOH+3H_2 \rightarrow RCH_3+2H_2O$	-88.0	-112.6
Decarbonylation:	$RCOOH+3H_2 \rightarrow RCH_3+2H_2O$	-59.5	49.7
Decarboxylation:	$RCOOH \rightarrow RH+CO_2$	-78.6	10.1
Gas-phase reaction	Equation	$\Delta G°_{533}$ [kJ mol^{-1}]	$\Delta H°_{533}$ [kJ mol^{-1}]
Methanation:	$CO + 3H_2 \rightarrow CH_4 + H_2O$	-88.4	-215.3
Methanation:	$CO_2 + 4H_2 \rightarrow CH_4 + 2H_2O$	-69.2	-175.7
Water-gas shift:	$CO + H_2O \rightarrow CO_2 + H_2$	-19.1	-39.6
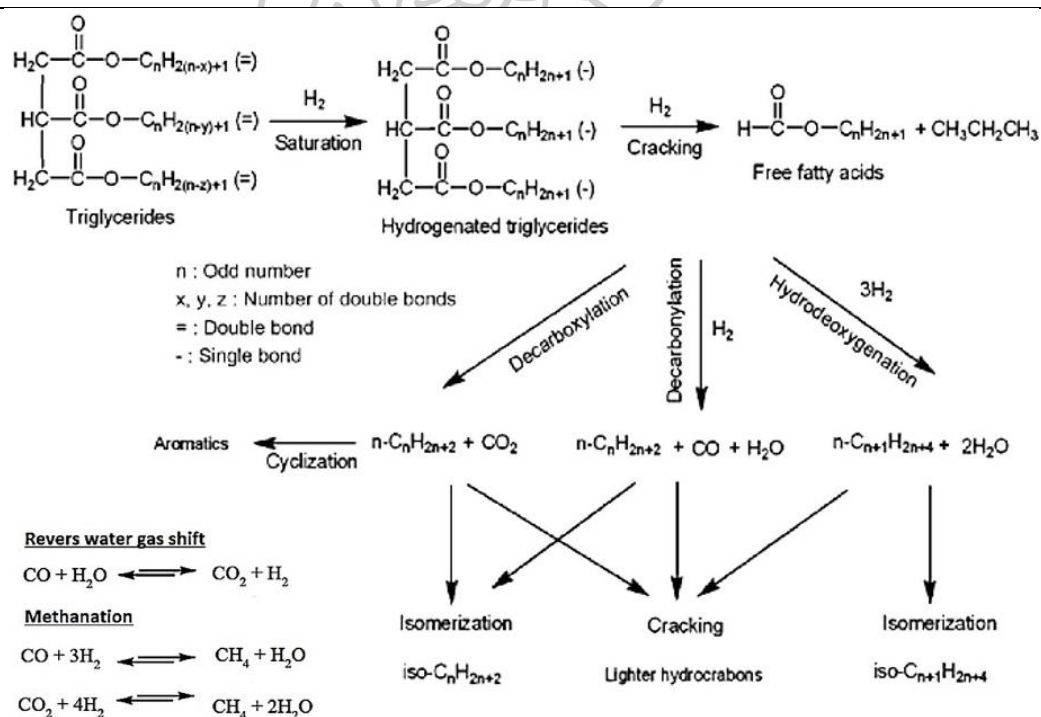
Figure 7 Reaction pathways for the hydroconversion of triglycerides into green diesel.

3.3 Palm refined process

Figure 8 shows the refinery process of palm oil. Firstly, crude palm oil (CPO) was degummed to as called degummed crude palm oil (DPO) by precipitation processes that use phosphoric acid as a precipitant. The DPO has removed impurity about pigment and trace metals, bleached palm oil (BPO) is obtained by bleaching. The BPO was then deodorized to refined, bleached, deodorized palm oil (RBDPO) and palm fatty acid distillate (PFAD) as a by-product. The RBDPO was fractionated to refined palm olein (RPO) and refined palm stearin (RPS). The composition of PFAD was shown in Table 4. Palmitic acid, oleic acid are the main components of palm feedstocks.
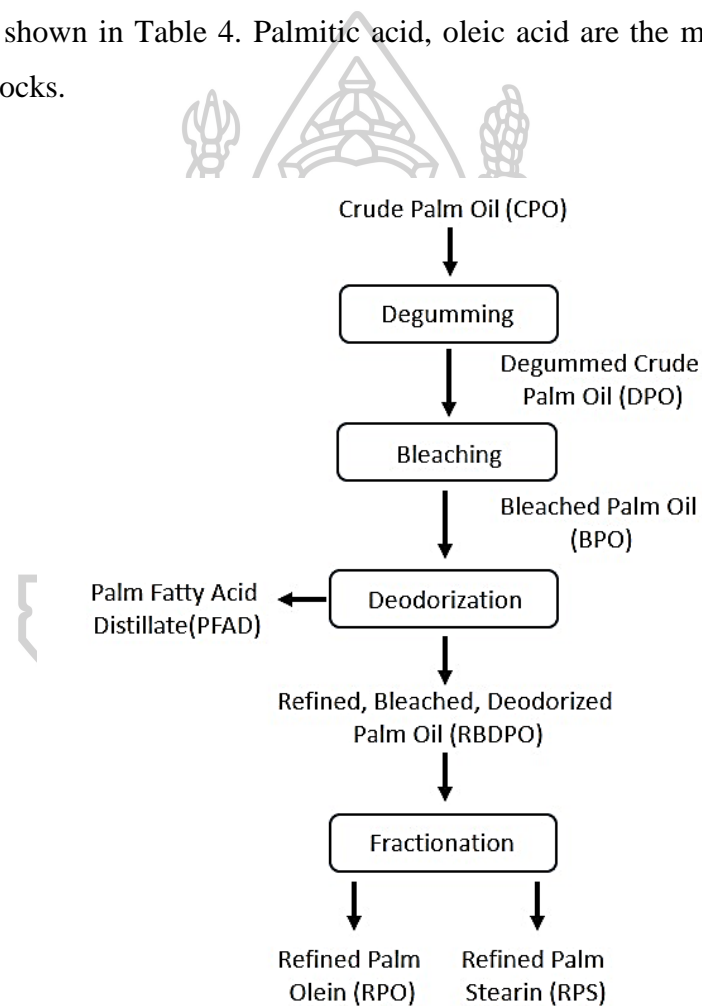
Figure 8 Physical refinering process of crude palm oil [42].

Table 4 The fatty acids composition of palm feedstock [12, 17, 19].

Fatty acid (wt.%)	PFAD	RPO	RPS
C 12:0 (Lauric acid)	-	0.4	-
C 14:0 (Myristic acid)	1.1	0.8	0.3
C 16:0 (Palmitic acid)	49.0	37.4	58.9
C 16:1 (Palmitoleic acid)	0.2	0.2	0.2
C 18:0 (Stearic acid)	4.1	3.2	4.7
C 18:1 (Oleic acid)	35.8	45.8	27.4
C 18:2 (Linoleic acid)	8.3	11.1	6.9
C 18:3 (Linolenic acid)	0.3	0.3	0.3
C 20:0 (Arachidic acid)	0.3	0.3	0.3
C 20:1 (*n*-9, Eicosenoic acid)	0.2	0.1	0.2
C 24:1 (Tetracosenoic acid)	0.6	-	0.8

3.4 Catalyst for hydrodeoxygenation

The catalyst in conventional hydroprocessing was nickel and molybdenum are a promoter and active site, respectively. The sulfided NiMo catalysts promote hydrodeoxygenation and decarbonylation as a reaction pathway. The bimetallic sulfide catalysts such as $NiMoS_2$, $CoMoS_2$, and $NiWS_2$ supported on zeolites, carbon, Al_2O_3, SiO_2, and TiO_2 are suitable for deoxygenation of triglycerides due to highly selective toward hydrodeoxygenation at a moderate temperature [6, 18]. Among them, supported $NiMoS_2$ catalysts showed the highest catalytic activity for the reaction. The type of support materials commonly utilized for the hydrotreating process is Al_2O_3. The Al_2O_3 is selected as a support material because of its moderate acidity and high surface area [43].

CHAPTER IV

METHODOLOGY

4.1 Chemical

The chemicals for use in this research was shown in Table 5.

Table 5 The details of chemicals used in the catalysts preparation and hydroprocessing process.

Chemicals	Formula	Grade	Manufacture
PFAD, RPO	-	-	Patum vegetable Thailand
Nickel nitrate	$Ni(NO_3)_2 \cdot 3H_2O$	Assay 97%	UNILAB
Ammonium molybdate	$(NH_4)_6Mo_7O_{24} \cdot 4H_2O$	Assay 81.0-83.0%	UNILAB
Copper	$Cu(NO_3)_2 \cdot 6H_2O$	Assay 99%	Merck
Aluminum oxide	$\gamma\text{-}Al_2O_3$	Assay 100%	Fluka
Zeolite	HZSM-5	Assay 100%	Riogen
Hydrogen	H_2	99.9%	Linde
Synthesis gas	CO/H_2 (30:70)	99.9%	Linde

4.2 Catalysts preparation

Before catalyst preparation, the support was crushed and sieved to 0.45-1.0 mm particle size. The NiMo was supported on commercial $\gamma\text{-}Al_2O_3$ via impregnation method by dropping the nickel nitrate solution and ammonium molybdate (2.4 wt.% of Ni and 9.4 wt.% of Mo) as a precursor of Ni and Mo, respectively. After impregnating, the catalyst was rest at room temperature for 6 h and dried on the oven at 110 °C for overnight. The catalyst was calcined for eliminating the impurity from

precursor by increasing the temperature from room temperature to 500 °C in the air with a ramping rate of 5 °C min^{-1} and hold at 500 °C for 5 h.

The NiCu/HZSM-5 catalyst was prepared by impregnating the solution of nickel nitrate and copper (II) nitrate (12.5 wt.% of Ni and 2.5 wt.% of Cu) on commercial HZSM-5 and dried at 110 °C and calcined at 550 °C for 5 h.

4.3 Catalysts characterization

4.3.1 X-ray diffraction

The X-ray diffraction (XRD) patterns of catalyst was obtained using an X-ray diffractometer, Siemens D5000. The experiments were performed with CuK$_\alpha$ radiation and over the 2θ ranges from 20° to 80°.

4.3.2 N$_2$ physisorption

The specific surface area and pore size diameter were determined from the N$_2$ physisorption technique by using a BEL SORP mini II device. To remove the moisture bound on the surface of catalyst by a pretreatment system at 220 °C for 3 h under 50 ml min^{-1} of helium gas flow. The specific surface area and pore volume were calculated by the BET method. The average pores size diameter of the catalysts were calculated from desorption isotherm branches by the BJH method.

4.3.3 Temperature programmed reduction

The reduction behavior and reducibility of catalysts were measured by the temperature programmed reduction (TPR) with 10 % H$_2$ in N$_2$. The 0.1 g of catalyst was pretreated at 150 °C for 2 h with heating rate of 10 °C min^{-1} under 30 ml min^{-1} of nitrogen gas flow. The analysis of hydrogen consumption was performed using a thermal conductivity detector (TCD).

4.3.4 Thermogravimetric analysis

The investigation of the coking behavior of the spent catalyst was measured by thermogravimetric analysis (TGA). The spent catalysts was heated up to 1000 °C with a heating rate of 10 °C min^{-1}.

4.4 Experimental

4.4.1 Catalysts activation

Before the reaction test the NiMo/γ-Al$_2$O$_3$ catalyst was activated by sulfidation. The 6 ml of the catalyst was loaded into the reactor. The catalyst was heated up to 400 °C with a ramping rate of 10 °C min^{-1} under 40 bar of hydrogen gas pressure with a liquid stream containing 3 wt.% CS$_2$ in *n*-heptane. The liquid stream add to the reactor at 150 °C with a flow rate 0.17 ml min^{-1} for 3 h

For the reduced NiMo/γ-Al$_2$O$_3$ catalyst, the NiMo/γ-Al$_2$O$_3$ after preparation which mostly in the oxide form was reduced at 700 °C for 2 h under H$_2$ flow. The NiCu/HZSM-5 catalyst was reduced at 450 °C for 2 h.

4.4.2 Catalyst deoxygenation reaction test

The hydroprocessing was carried out in a continuous fixed-bed reactor. The schematic diagram of the experimental apparatus is shown in Figure 9. The reactor made from stainless steel tube with an internal diameter of 0.9 cm. PFAD was externally heated to liquid phase before introducing to the reactor by high-pressure pump while reactant gases can be introduced using mass flow controllers.

4.4.3 FTIR

The functional group of the feedstock and liquid products were identified by the Fourier transform infrared (FTIR) spectroscopy (Perkin Elmer spectrum GXFT-IR).

4.4.4 Analysis of liquid and gas products

The liquid phase was analyzed by gas chromatograph equipped with flame ionization detector (GC-FID). The operating condition are shown in the Table 6. The offline Shimadzu GC-14B gas chromatograph was equipped with DB-1HT column (30 m x 0.32 mm x 0.1 μm). Simulated distillation (ASTM D2887) was employed to determine the boiling point range for each fractions. The conversion and product selectivity can be calculated as follows.

$$\text{Conversion (\%)} = \frac{\text{Feed}_{FA+TG} - \text{Product}_{FA+TG}}{\text{Feed}_{FA+TG}} \times 100$$

Where

Feed_{FA+TG} is the weight percent of fatty acid and triglyceride in feed.

Product_{FA+TG} is the weight percent of fatty acid and triglyceride in product.

$$\text{Gasoline selectivity (\%)} = \frac{\text{Product}_{C_5-C_{11}} - \text{Feed}_{C_5-C_{11}}}{\text{Feed}_{FA+TG} - \text{Product}_{FA+TG}}$$

$$\text{Diesel selectivity (\%)} = \frac{\text{Product}_{C_{12}-C_{18}} - \text{Feed}_{C_{12}-C_{18}}}{\text{Feed}_{FA+TG} - \text{Product}_{FA+TG}}$$

Where

$\text{Feed}_{C_5-C_{11}}$ is the weight percent of alkanes at a boiling point in range of C_5-C_{11} in feed.

$\text{Product}_{C_5-C_{11}}$ is the weight percent of alkanes at a boiling point in range of C_5-C_{11} in product.

$\text{Feed}_{C_{12}-C_{18}}$ is the weight percent of alkanes at a boiling point in range of C_{12}-C_{18} in feed.

$\text{Product}_{C_{12}-C_{18}}$ is the weight percent of alkanes at a boiling point in range of C_{12}-C_{18} in product.

$$\text{Oil phase fraction} = \frac{\text{weight of oil phase product}}{\text{weight of feed}}$$

$$\text{Gas fraction} = 1 - \frac{\text{weight of oil phase product}}{\text{weight of feed}}$$

Gasoline yield = oil phase fraction x conversion x gasoline selectivity

Diesel yield = oil phase fraction x conversion x diesel selectivity

Yield of liquid fuel = diesel yield + gasoline yield

The gaseous phase was analyzed by gas chromatography equipped with thermal conductivity detector (GC-TCD) which their operating condition are shown in the Table 7.

Table 6 Operating condition in Gas Chromatography – Flame Ionization Detector (GC-FID).

Gas chromatograph	Condition
Detector	FID
Column	DB-1HT
Carrier gas	He
Split	30 ml min^{-1}
Purge	4 ml min^{-1}
Make up pressure	40 kPa
Carrier pressure	40 kPa
Detector temperature	370 °C
Column temperature	40 °C ramp 8 °C min^{-1} to held at 270 °C for 11 min, and increase of 15 °C min^{-1} to 370 °C and held for 15 min
Injector temperature	340 °C

Table 7 Operating condition in Gas Chromatography–Thermal Conductivity Detector (GC-TCD).

Gas chromatograph	Condition
Detector	TCD
Column	Porapak Q
Carrier gas	Ar (30 ml min^{-1})
Make up pressure	40 kPa
Carrier pressure	Ar 40 kPa
Detector temperature	150 °C
Column temperature	40 °C ramp 20 °C min^{-1} to held at 100°C for 11 min
Injector temperature	150 °C
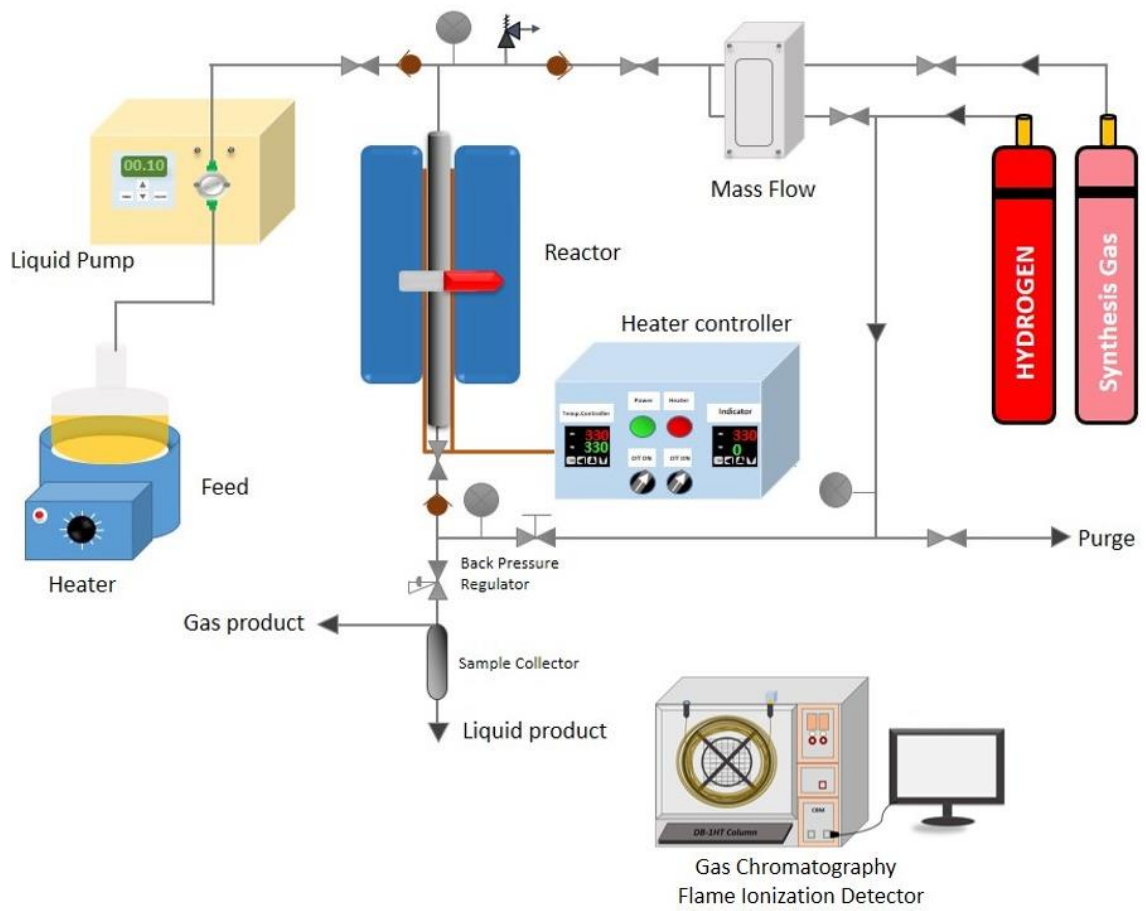
Figure 9 Illustration of the fixed-bed reactor and controller in continuous process.
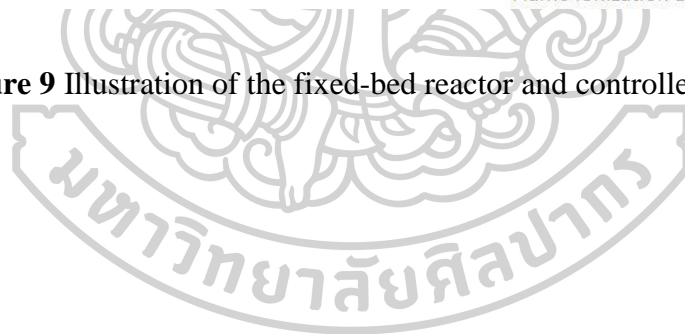
CHAPTER V

RESULTS AND DISCUSSION

5.1 Catalyst characterization

5.1.1 X-ray diffraction

The X-ray diffraction (XRD) patterns of calcined NiCu/HZSM-5, calcined NiMo/γ-Al$_2$O$_3$, and sulfided NiMo/γ-Al$_2$O$_3$ catalyst were shown in Figure 10. In case of NiMo/γ-Al$_2$O$_3$ catalyst, the peaks at 32.60°, 38.49°, 46.71°, 56.76°, 61.37°, 67.94° and 77.29° corresponding to the (220), (222), (400), (422), (511), (440) and (621) phase assigned to γ-Al$_2$O$_3$ support catalyst with cubic structure [32, 44-46]. The crystalline of MoO$_3$ cannot be observed in this result because Mo was highly dispersed on high surface area of the support. Moreover, the presence of crystalline NiMoO$_4$ is not evident by XRD [47-49]. NiO, Ni$_2$O$_3$, and NiAl$_2$O$_4$ cannot be detected by XRD because the peak is an amorphous phase and overlap with the peaks of γ-Al$_2$O$_3$ [50]. On the other hand, the peak of MoS$_2$ was found in the XRD pattern of sulfide catalyst at 33.5° and 58° corresponding to the (100) and (110) phase [51-54]. The XRD pattern of the NiCu/HZSM-5 catalyst shown in Figure 10 (a). The peaks of the HZSM-5 shown at 23.0° and 23.8° are corresponding to [303] and [503], respectively. In this case, was founded formation of a metal oxide including NiO and CuO. The peak of NiO was show at 37.1°, 43.1°, 62.6°, 75.3° and 79.1° corresponding to [111], [200], [220], [311] and [222], respectively. The CuO at 2θ of 37.1 and 43.1 are assignable to [111] and [220], respectively [26].
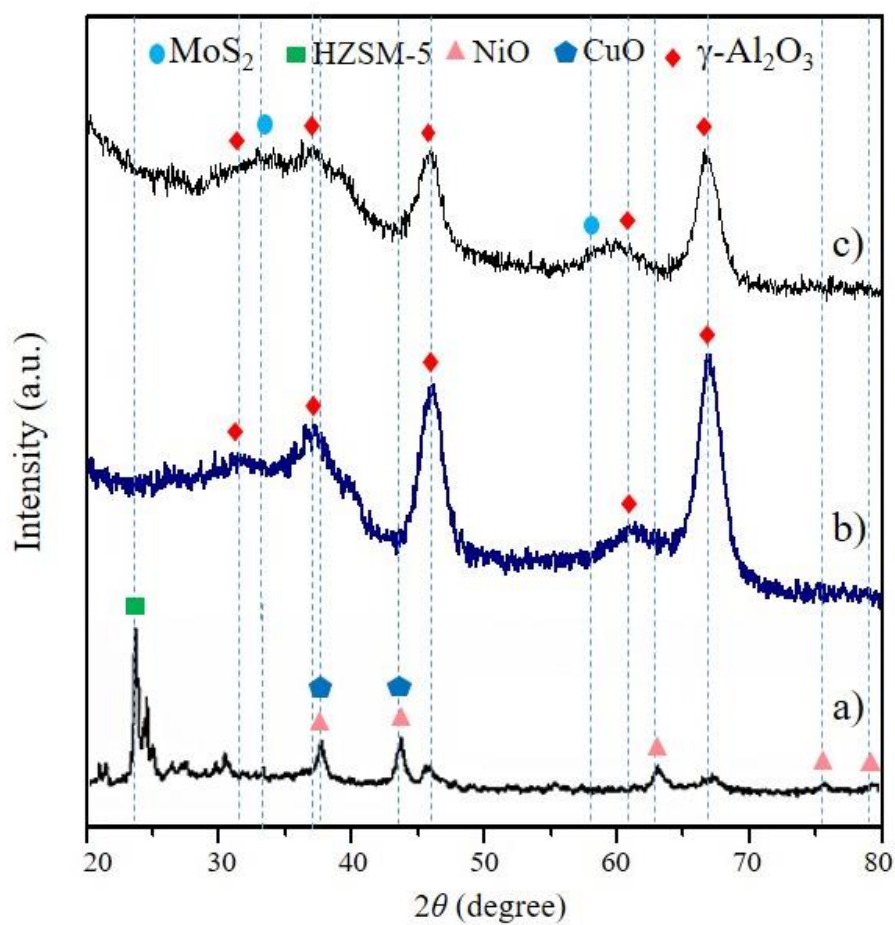
Figure 10 The XRD patterns of a) calcined NiCu/HZSM-5 and (b) calcined NiMo/γ-Al₂O₃ and c) sulfided NiMo/γ-Al₂O₃ catalyst.

5.1.2 N$_2$ Physisorption

N$_2$ adsorption-desorption measurements were conducted to examine the textural properties of the catalysts. Table 8 summarizes the specific surface area, pore volume, and mean pore diameter of the synthesized samples. The specific surface area of bare γ-Al$_2$O$_3$ and HZSM-5 are 232 m^2 g^{-1} and 292 m^2 g^{-1}, respectively. The high specific surface area of the supports allows very high dispersions and loadings of the active phase [55].

The specific area and total pore volume decreased by impregnation of Ni and Mo metal on γ-Al$_2$O$_3$ support. This might be due to partial pore blocking. [56].

The adsorption-desorption isotherm of NiMo/γ-Al$_2$O$_3$ and NiCu/HZSM-5 shown in Figure 11. It was found that NiMo/γ-Al$_2$O$_3$ catalyst exhibited type IV isotherm while NiCu/HZSM-5 catalyst exhibited type I isotherm [57]. In the case of NiMo/γ-Al$_2$O$_3$ indicated the characteristic of the mesoporous structure and pore sizes of catalyst in the range of 11-13 nm [58].
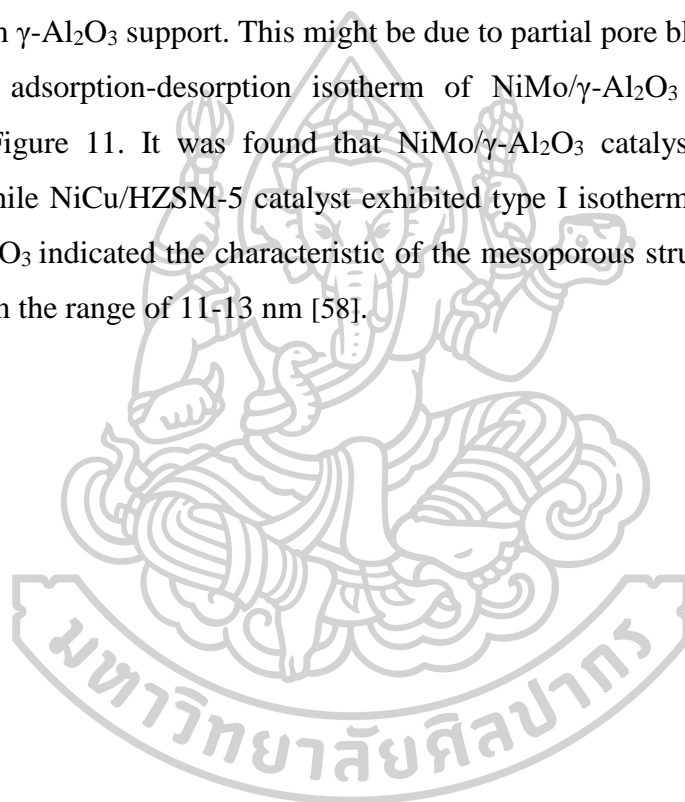
Table 8 Physicochemical properties of the calcined catalysts.

Catalysts	Surface area[a] $(m^2\,g^{-1})$	Total pore[b] volume $(cm^3\,g^{-1})$	Micropore[c] volume $(cm^3\,g^{-1})$	Mean pore[d] diameter (nm)
γ-Al$_2$O$_3$	232	0.73	-	12.58
NiMo/γ-Al$_2$O$_3$	175	0.54	-	11.01
HZSM-5	292	0.26	0.19	4.65
NiCu/HZSM-5	276	0.25	0.18	4.37

[a] Specific BET surface area obtained from nitrogen adsorption isotherm.

[b] Total pore volume obtained at $P/P_0 = 0.95$.

[c] Microspore measured by MP plot method.

[d] Mean pore diameters obtained from BET method.
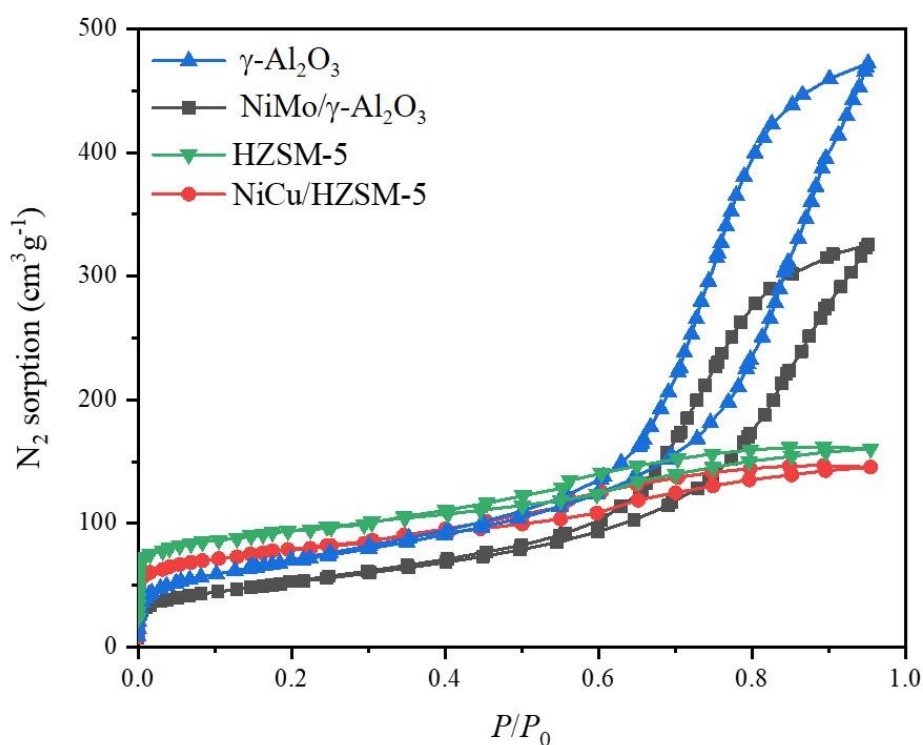
Figure 11 Nitrogen adsorption/desorption isotherm of pure γ-Al$_2$O$_3$, NiMo/γ-Al$_2$O$_3$, pure HZSM-5 and NiCu/HZSM-5 catalysts.

5.1.3 Temperature programmed reduction

The temperature programmed reduction of NiMo/γ-Al$_2$O$_3$ and NiCu/HZSM-5 catalyst are shown in Figure 12. The H$_2$-TPR experiments were employed to investigate the reducibility, and the interaction between metal species and the support in the catalysts. The result shows the H$_2$ reduction temperature of 200 °C to 300 °C related to the reduction of Cu^{2+} to Cu [59]. The reduction of Ni was similar in both catalysts. The Ni^{2+} was reduced to Ni at 400 °C [61]. However, [60] found a broad peak of reduction of bulk NiO species in a range between 300 °C to 500 °C. Moreover, the temperature of 500 °C to 600 °C are corresponding to the reduction of a cationic form of nickel (NiSiO$_3$) and the small NiO particles inside the pore of support [62]. Besides, the case of NiMo/γ-Al$_2$O$_3$ catalyst found that the reduction temperature of NiMoO$_4$ and MoO$_3$ was at above 600 °C [63]. The results indicated nickel strong interaction with γ-Al$_2$O$_3$ than the HZSM-5 support catalyst presented in a shift temperature reduction of NiO.
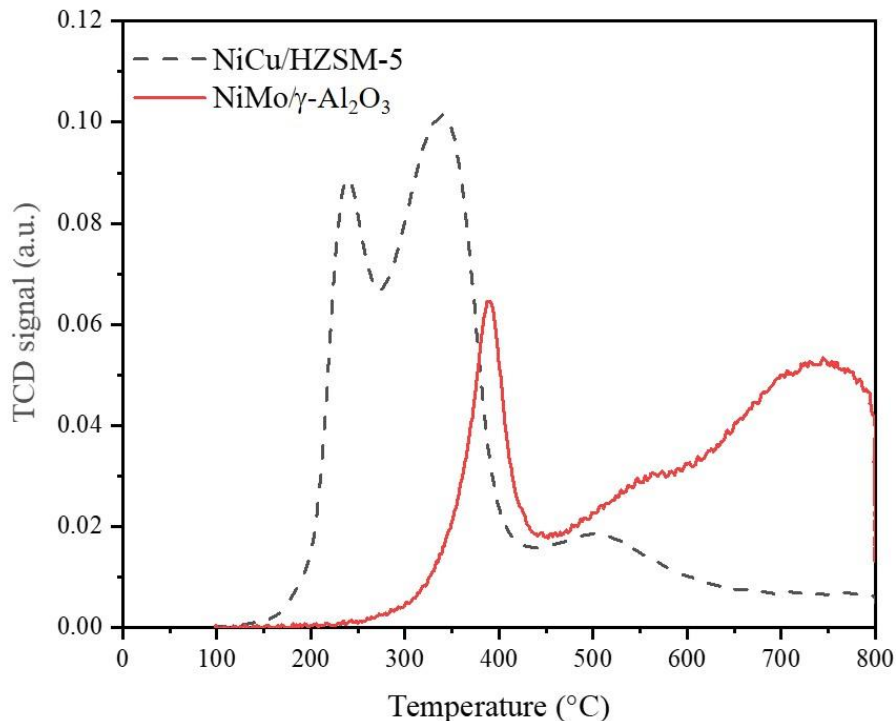
Figure 12 Hydrogen-temperature programed reduction (H$_2$-TPR) profile of NiMo/γ-Al$_2$O$_3$ and NiCu/HZSM-5 catalysts.

5.2 Hydrotreating process

The NiMo supported on γ-Al$_2$O$_3$ was investigated to estimate the activity of the catalyst including conversion selectivity and yield of diesel. Besides, the effect of continuously hydrotreated parameters including reaction temperature, reaction pressure, liquid hourly space velocity, and gas/feed ratio were also studied to obtain optimal condition for maximizing diesel yield.

5.2.1 Synthesis gas versus hydrogen on the reaction performance.

5.2.1.1 Using refined palm olein (RPO) as a feedstock

First, refined palm oil or RPO (edible-oil) was employed as a type of triglyceride feedstock. The triglyceride conversion under the operating pressure of synthesis gas and pure hydrogen are shown in Figure 13 and Table 9. The results show that the conversion and diesel yield increase when increase pressure. As shown by the dashed line in Figure 13, the maximums theoretical yield without other side reactions are 80.5% and 85.5% for DCO$_x$ and HDO reaction pathways, respectively. The obtained yield from the experiment approached to these values and will be discussed later.

The results showed that n-C$_{16}$ and n-C$_{18}$ (n-C$_n$) were the main component over the range of operating pressure and gas/feed ratio (Figure 14 and Table 9). The n-C$_{n-1}$/ n-C$_n$ decreased when increasing hydrogen pressure. The increased of n-C$_{n-1}$/ n-C$_n$ may slightly decreased the diesel yield as the pathway of n-C$_{n-1}$ offer lower diesel yield as demonstrated by the different in their maximum theoretical yield

The containing of triglyceride feedstock in the liquid product was characterized by functional analysis (Figure 15). The adsorption peak at 1743 cm^{-1} and 115 0 cm^{-1} in the FTIR spectrum was assigned to *aliphatic* ester bonds -C=O stretching and -C-O- stretching, respectively [64, 65]. The non-detected of the *aliphatic* ester bonds in hydrotreated products confirms complete conversion of triglycerides.

The gas products can be obtained in hydrotreated triglyceride feedstock including C$_3$H$_8$, CO, CO$_2$, and CH$_4$. From figure 16, the CO was found as a major gas product of both operating atmosphere. While CH$_4$ was observed from the high pressure of synthesis gas. The C$_3$H$_8$ is not presented in a gas product which might because the C-C cracking is possible.

The thermogravimetric analysis of the spent catalysts was shown in Figure 20, which observed at a temperature of 50 °C to 100 °C, 200 °C to 300 °C, and 300 °C to 500 °C, which correspond to the loss of moisture, soft coke, and hard coke, respectively [67]. The comparison of catalyst activity between synthesis gas and pure hydrogen was analyzed by thermogravimetric analysis. It's indicating that coke formation of spent NiMo/γ-Al$_2$O$_3$ by synthesis gas slightly higher than pure hydrogen.
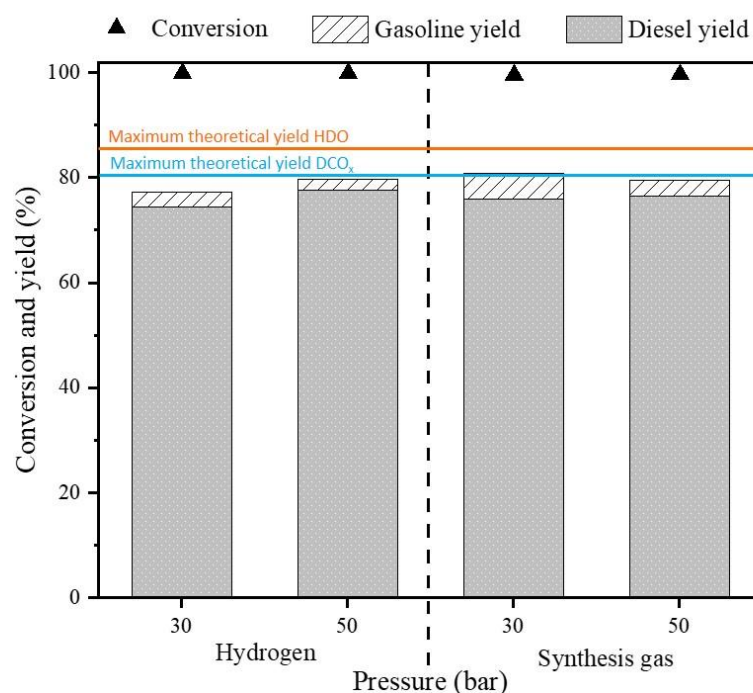
Figure 13 The effect of operating pressure and gas/feed ratio on RPO conversion and yield of sulfided NiMo/γ-Al$_2$O$_3$ catalyst under operating pressure of (a) pure hydrogen and (b) synthesis gas. The reactions performed at operating temperature = 330 °C, gas/feed ratio = 1000 (v/v) and liquid hourly space velocity (LHSV) = 1 h^{-1}.
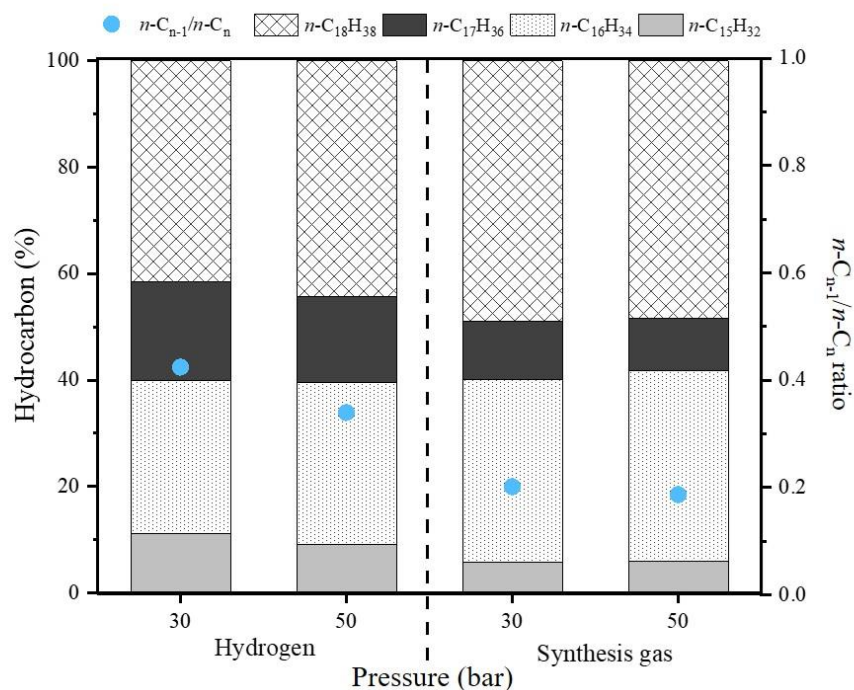
Figure 14 The effect of operating pressure and gas/feed ratio on *n*-alkanes distribution under operating pressure of (a) pure hydrogen and (b) synthesis gas. The reactions were performed by RPO feedstock over sulfided NiMo/γ-Al$_2$O$_3$ catalyst at operating temperature = 330 °C, gas/feed ratio = 1000 (v/v) and liquid hourly space velocity (LHSV) = 1 h^{-1}.

Table 9 Comparison of refined palm olein (RPO) conversion, diesel yield and C$_{n-1}$/C$_n$ ratio or (*n*-C$_{15}$+*n*-C$_{17}$)/(*n*-C$_{16}$+*n*-C$_{18}$) over sulfided NiMo catalysts supported on alumina (Operating temperature = 330 °C, gas/feed ratio = 1000 and LHSV = 1 h^{-1}).

Sample	Conversion (%)	Diesel yield (%)	C$_{n-1}$/C$_n$ ratio
Pure hydrogen			
30 bar	99.8	74.5	0.42
50 bar	99.8	77.7	0.34
Synthesis gas			
30 bar	99.5	75.8	0.2
50 bar	99.8	76.4	0.18
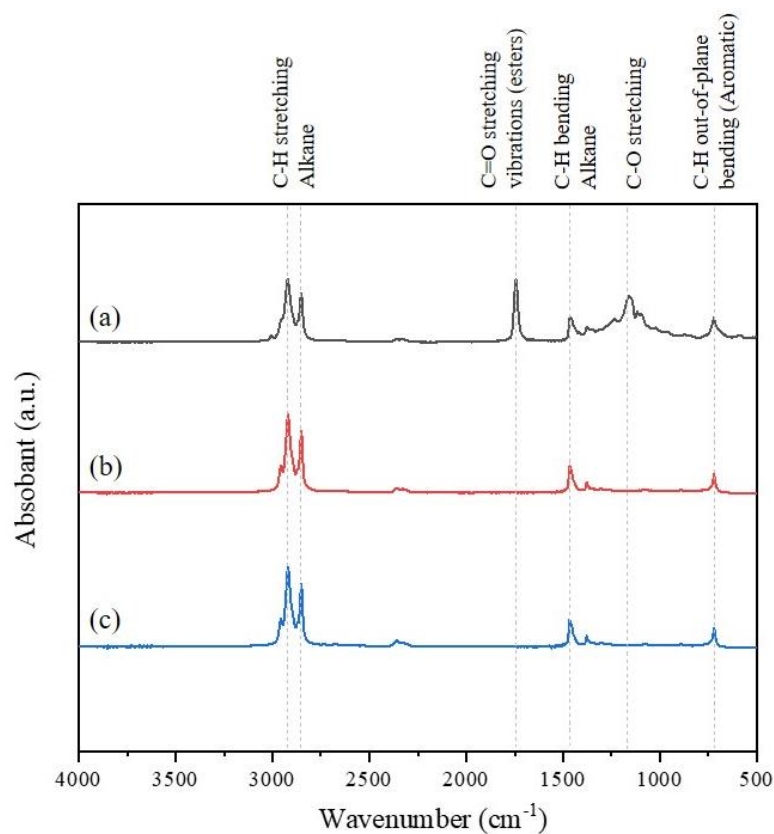
Figure 15 The FTIR spectrums of (a) refined palm olein (RPO). The hydrotreating reaction performed over sulfided NiMo/γ-Al$_2$O$_3$ under pressure of (b) pure hydrogen, and (c) synthesis gas. (Operating temperature = 330 °C, pressure = 50 bar, gas/feed ratio = 1000 (v/v) and LHSV = 1 h^{-1}).

Figure 16 The effect of operating pressure and gas/feed ratio on mole fraction of gaseous products under operating pressure of (a) pure hydrogen and (b) synthesis gas. The reactions were performed by RPO feedstock over sulfided NiMo/γ-Al$_2$O$_3$ catalyst at operating temperature = 330 °C, gas/feed ratio = 1000 v/v and liquid hourly space velocity (LHSV) = 1 h^{-1}.
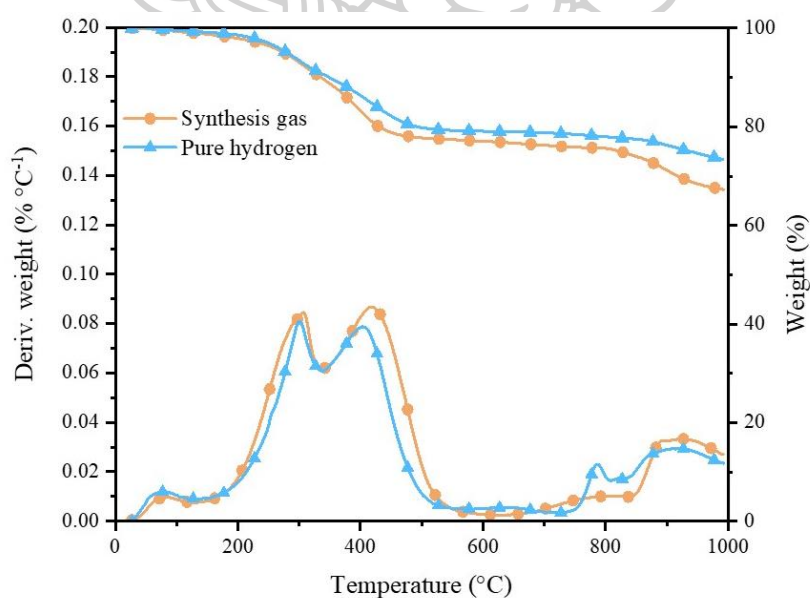
Figure 17 Thermogravimetric analysis of spent NiMo/γ-Al$_2$O$_3$ catalysts. The operating condition at 50 bar of pure hydrogen and synthesis gas, temperature of 330 °C, LHSV = 1 h^{-1}, gas/feed ratio = 1000 v/v by RPO feedstock.

In the next section, palm fatty acid distillate is employed to elucidate the effect from feedstock that free fatty acid is different from triglyceride feedstock in the previous section or not. In addition, PFAD which is a by-product and inedible is more attractive than edible RPO which is also costly.

5.2.1.2 Using palm fatty acid distillate (PFAD) as a feedstock

The effect of operating pressure and gas/feed ratio on conversion and diesel yield is shown in Figure 18. The effect of pressure was studied in the range of 30 and 50 bar while the gas/feed ratio was varied in the range of 250-1000 v/v. The conversion of palm fatty acid distillate feedstock was slightly increased when increased the gas/feed ratio. The complete conversion of can be obtained under both pure hydrogen and synthesis gas pressures as shown in Figure 18 a) and b), respectively. At the highest operating pressure and gas/feed ratio, the highest diesel yield was obtained from H_2 approximately 84.6% while the highest diesel yield from synthesis gas was 80.2%. The behavior of both pressured gas on converted palm fatty acid distillate feedstock and diesel yield is no different.

It is worth to note that the maximum theoretical yields of deoxygenated products based on 6.8 wt.% of triglyceride and 93.2 wt.% of free fatty acid with fatty acid composition (Table 4) containing in PFAD can be calculated. The maximum theoretical yields, without other side reactions, are 83.7% and 88.9% for DCO_x and HDO reaction pathway, respectively. The results showed the diesel yield obtained from sulfided $NiMo/\gamma\text{-}Al_2O_3$ catalyst could approach the maximum theoretical yield.

The effect of operating pressure and gas/feed ratio on liquid product distribution are shown in Figure 19 and Table 10. The main components of n-alkane were $n\text{-}C_{16}$ and $n\text{-}C_{18}$ that have the same carbon atom corresponding to palm fatty acid distillate feedstock. In both operating gas, the $n\text{-}C_{n-1}$ decreasing when increasing pressure and gas/feed ratio. Although the increase of $n\text{-}C_{15}$ and $n\text{-}C_{17}$ or $n\text{-}C_{n-1}$ can cause a decrease in diesel yield, some contribution from cracking reaction is possible.

When compared between pure hydrogen and synthesis gas, it was found that the synthesis gas promotes $n\text{-}C_n$ more than pure hydrogen at the same operating pressure. This is because the carbon monoxide in the synthesis gas act as a reducer to produce $n\text{-}C_n$ [12]. The results show the $n\text{-}C_{n-1}/n\text{-}C_n$ decreased with increasing

gas/feed ratio because HDO is more favor. The effect of gas/feed ratio on n-C_{n-1}/n-C_n is less pronounced with increasing the pressure to 50 bar. This might be because the amount of H_2 contacting with liquid reactant and catalyst are much in excess.

The gas products which obtained from catalytic deoxygenation and possible side reaction in gas phase (e.g. methanation and reverse water gas shift) is shown in Figure 20. The significant difference in CH_4 formation between the pure H_2 (Figure 20a) and syngas (Figure 20b) conditions implied that methanation between CO and H_2 could be occurred under this operating condition. Independent experiment on gas phase reaction was therefore performed by feeding with syngas (without PFAD) into sulfided $NiMo/\gamma$-Al_2O_3 catalyst bed. As shown in Figure 21, the gas composition is very similar to that obtain from hydroprocessing of PFAD. This result implied that apart from gas formation from deoxygenation process, the reaction among gas product catalyzed by sulfided $NiMo/\gamma$-Al_2O_3 catalyst under the operating condition affect significant on gas product distribution.

As shown in Figure 20b, the fraction of methane in gas product is more pronounced with increasing syngas pressure. This is because, in general, a higher pressure is favorable for the enhancement of the methanation reaction. However, the extent of gas phase reaction decreased with increasing gas flow rate (accompanied with increasing gas/feed ratio) due to lower residence time. Similar tendency on the effect of pressure and gas/feed ratio on gas phase reaction for pure H_2 gas condition but of course in smaller extent (Figure 21a).
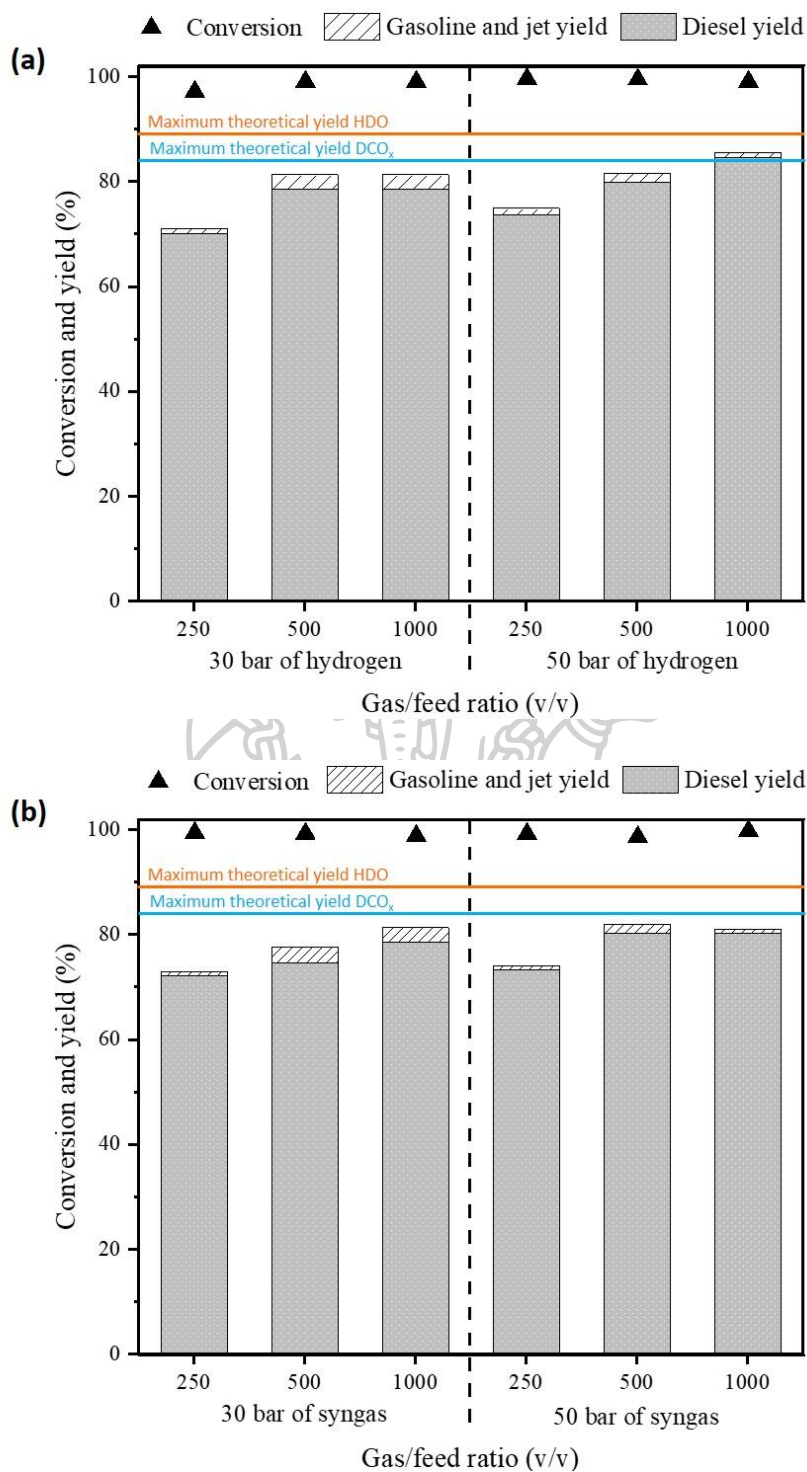
Figure 18 The effect of operating pressure and gas/feed ratio on PFAD conversion and yield of sulfided NiMo/γ-Al$_2$O$_3$ catalyst under operating pressure of (a) pure hydrogen and (b) synthesis gas. The reactions performed at operating temperature = 330 °C and liquid hourly space velocity (LHSV) = 1 h^{-1}.
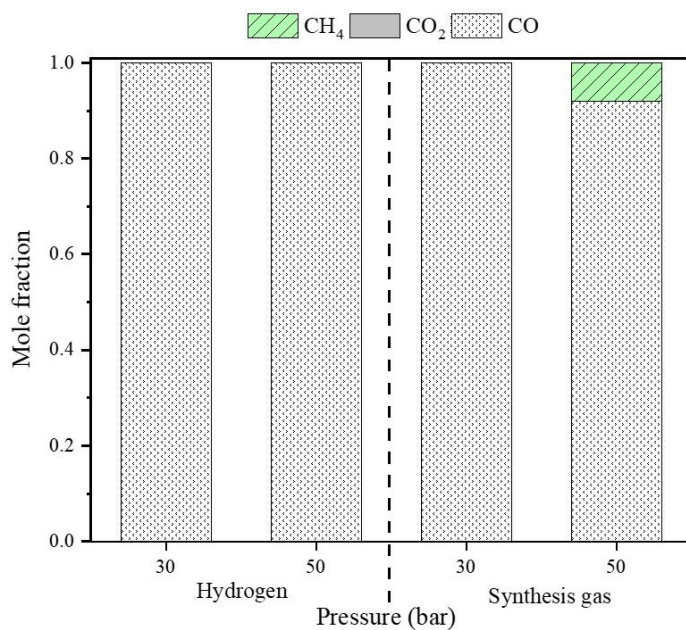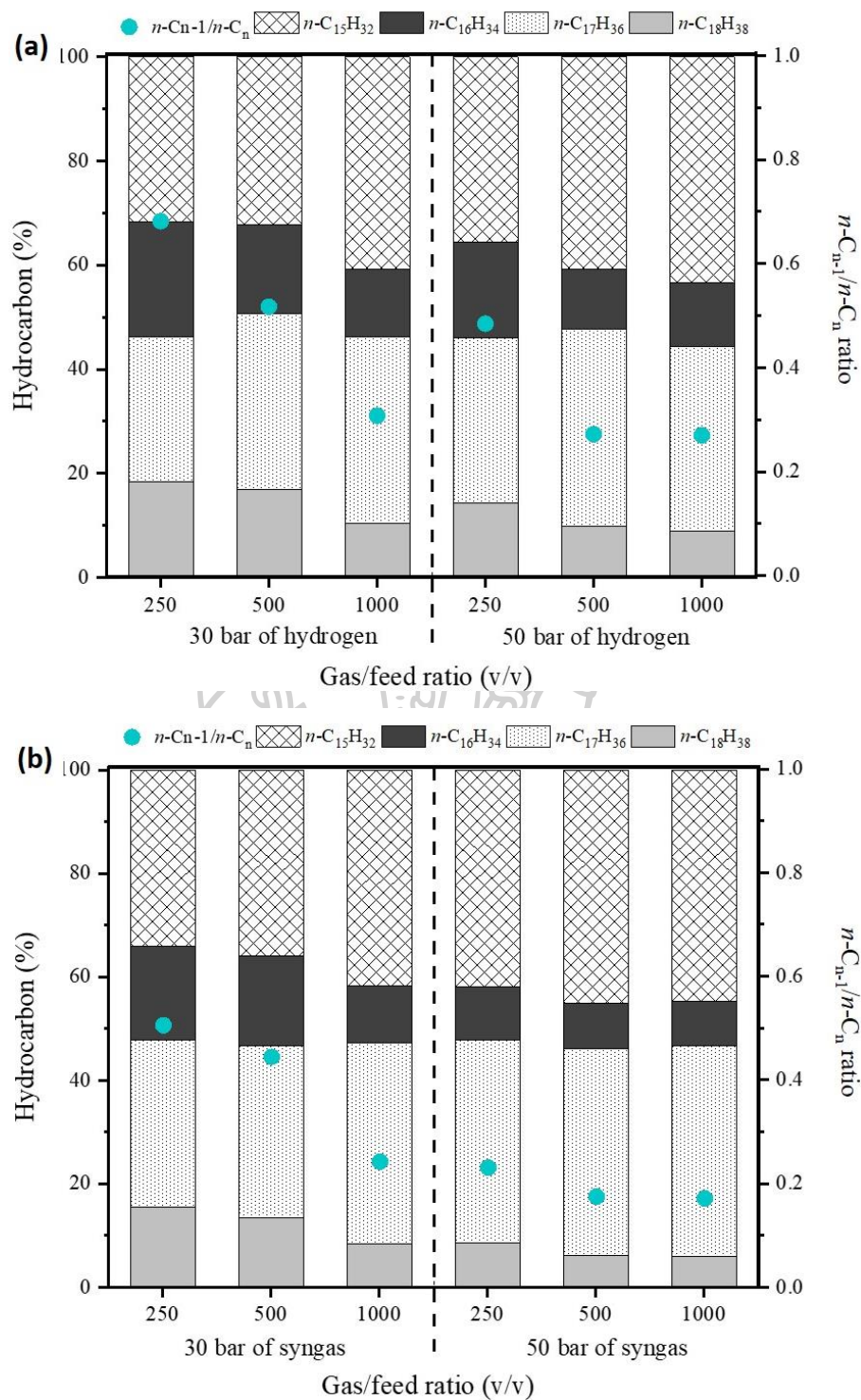
Figure 19 The effect of operating pressure and gas/feed ratio on *n*-alkanes distribution under operating pressure of (a) pure hydrogen and (b) synthesis gas. The reactions were performed by PFAD feedstock over sulfided NiMo/γ-Al$_2$O$_3$ catalyst at operating temperature = 330 °C and liquid hourly space velocity (LHSV) = 1 h^{-1}.
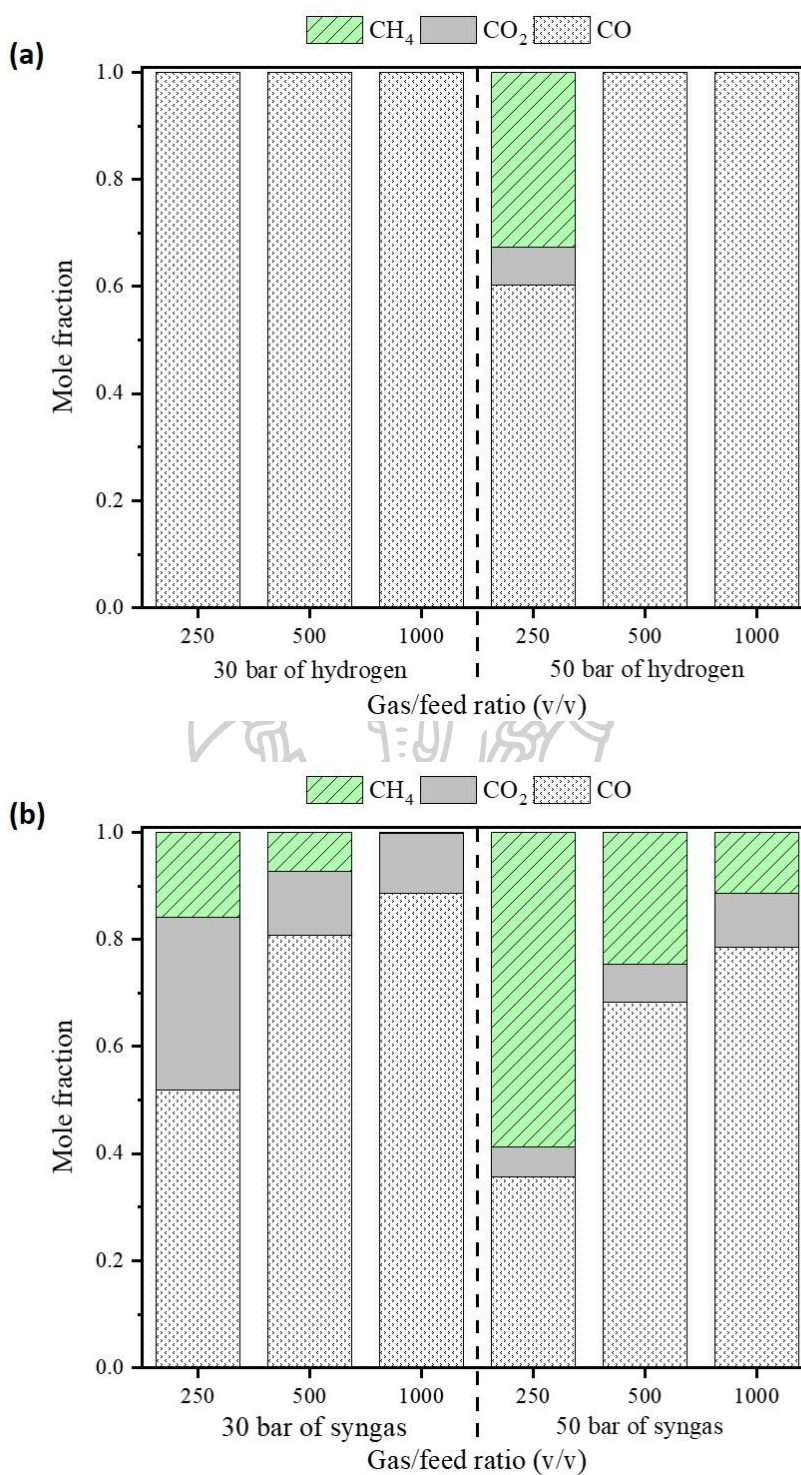
Figure 20 The effect of operating pressure and gas/feed ratio on mole fraction of gaseous products under operating pressure of (a) pure hydrogen and (b) synthesis gas. The reactions were performed by PFAD feedstock over sulfided NiMo/γ-Al$_2$O$_3$ catalyst at operating temperature = 330 °C, gas/feed ratio = 1000 v/v and liquid hourly space velocity (LHSV) = 1 h^{-1}.

Table 10 The *n*-alkane liquid products distribution over sulfided NiMo catalysts supported on alumina (Operating temperature = 330 °C and LHSV = 1 h^{-1}).

Sample	Fraction (%)				C_n	C_{n-1}
	n-C$_{15}$	*n*-C$_{16}$	*n*-C$_{17}$	*n*-C$_{18}$		
30 bar of pure hydrogen						
250 v/v	18.4	27.7	22.1	31.8	59.5	40.5
500 v/v	17.0	33.7	17.1	32.2	65.9	34.1
1000 v/v	10.4	35.7	13.1	40.8	76.5	23.5
50 bar of pure hydrogen						
250 v/v	14.3	31.8	18.3	35.5	67.3	32.6
500 v/v	9.8	37.9	11.6	40.7	78.6	21.4
1000 v/v	8.9	35.4	12.3	43.3	78.7	21.2
30 bar of synthesis gas						
250 v/v	15.4	32.4	18.2	34.0	66.4	33.6
500 v/v	13.4	33.3	17.3	35.9	69.2	30.7
1000 v/v	8.4	38.7	11.1	41.7	80.4	19.5
50 bar of synthesis gas						
250 v/v	8.5	39.3	10.2	42.0	81.3	18.7
500 v/v	6.1	40.0	8.8	45.1	85.1	14.9
1000 v/v	6.1	40.6	8.6	44.7	85.3	14.7
50 bar of pure carbon monoxide						
500 v/v	0	22.4	6.0	71.5	94.0	6.0
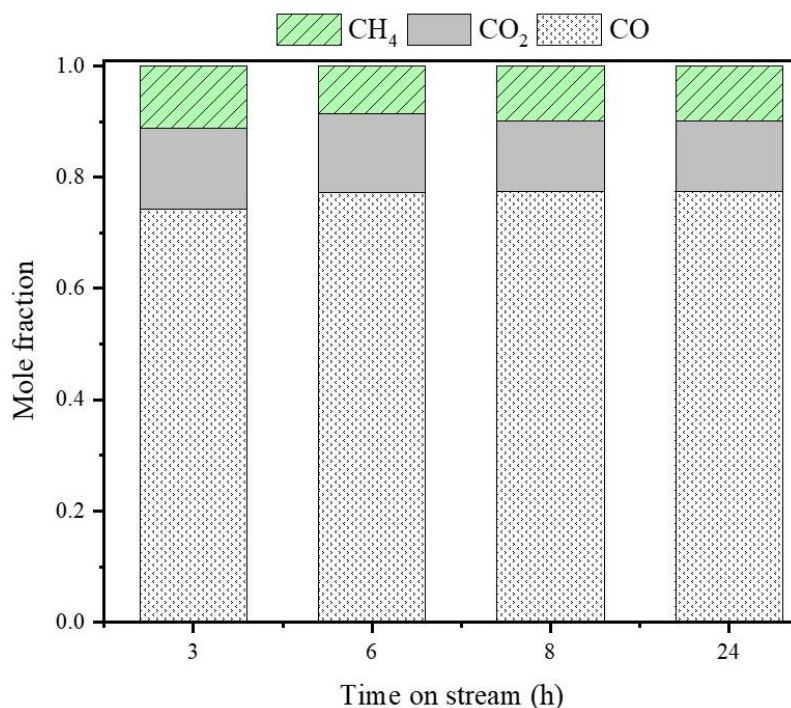
Figure 21 The mole fraction of gaseous productthe of sulfided NiMo/γ-Al$_2$O$_3$ catalyst under synthesis gas. The gas-phase reactions were performed at operating temperature = 330 °C, gas/feed ratio = 1000 v/v and liquid hour space velocity (LHSV) = 1 h^{-1}.

Moreover, to study the effect of operating gas via hydrotreating process over sulfided NiMo/γ-Al$_2$O$_3$ catalyst by operating under pure carbon monoxide, pure hydrogen, and synthesis gas. The results indicating that (Figure 22) the diesel yield from pure hydrogen and synthesis gas are stable approximately 80% in 42 h. On the other hand, the diesel yield from pure carbon monoxide rapid drop from 75% to 45% in 24 h.

Figure 23 shows that the highest conversion of palm fatty acid distillate feedstock indicated at 85% and dramatically dropped to 50% within 24 h of operating. Besides, the diesel yield decreased with a decrease in feed conversion. While the diesel selectivity remained stable at 98%. The results shown under different operating pressure on yields of hydrocarbon were concluded in Table 11. In the case of synthesis gas, the liquid product contained a number of *iso*-C$_{15}$-C$_{18}$ than pure hydrogen. The liquid product characterization under pure carbon monoxide cannot

complete converted palm fatty acid distillate feedstock. Moreover, the liquid product mainly *iso*-C_{15}-C_{18} (approximately 83%) and a high amount of molecule lighter than *n*-C_{15}.

To confirm the elimination of oxygen atoms in vegetable oil and fatty acids, the functional group of the liquid products were characterized by Fourier transform infrared (FTIR) spectroscopy (See in Figure 24). The adsorption peak at 1704 cm^{-1} in the FTIR spectrum corresponds to the carboxylic functional group of fatty acid [66] , which dominant in palm fatty acid distillate feedstock. Moreover, other peaks such as aromatic compounds (C-H out-of-plane bending peak at 722.5 cm^{-1}), alkene (C=C stretching peak at 838.5 cm^{-1}) and intermediate product such as alcohol, ester, ether (C-O stretching, O-H ending peak at 1286 cm^{-1}) were found in palm fatty acid distillate feedstock. The hydrotreating of palm fatty acid distillate under pure hydrogen and synthesis gas leads to *n*-alkane as shown by clearly the peak of fatty acid. While the peak of fatty acid (carboxylic group) can be observed in a liquid product that operating under carbon monoxide.

Although the hydrotreating process over sulfided NiMo/γ-Al_2O_3 catalyst cannot operate under pure carbon monoxide it shows isomerization and alkene formation resulting in liquid product characterization.
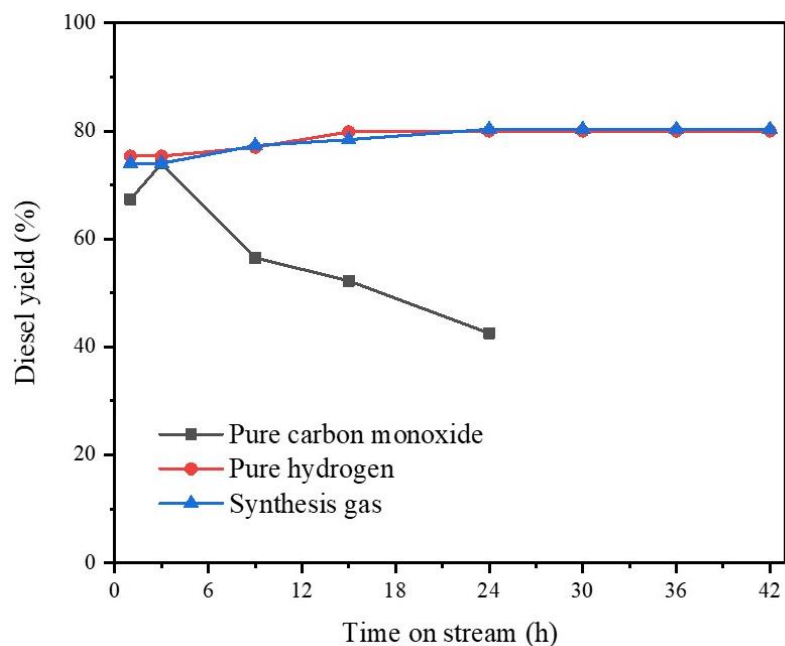
Figure 22 The diesel yield of sulfided NiMo/γ-Al$_2$O$_3$ catalyst under pure carbon monoxide, pure hydrogen and synthesis gas (PFAD feedstock), operating temperature = 330 °C, pressure = 50 bar, LHSV = 1 h^{-1} and gas/feed ratio = 500 (v/v)).
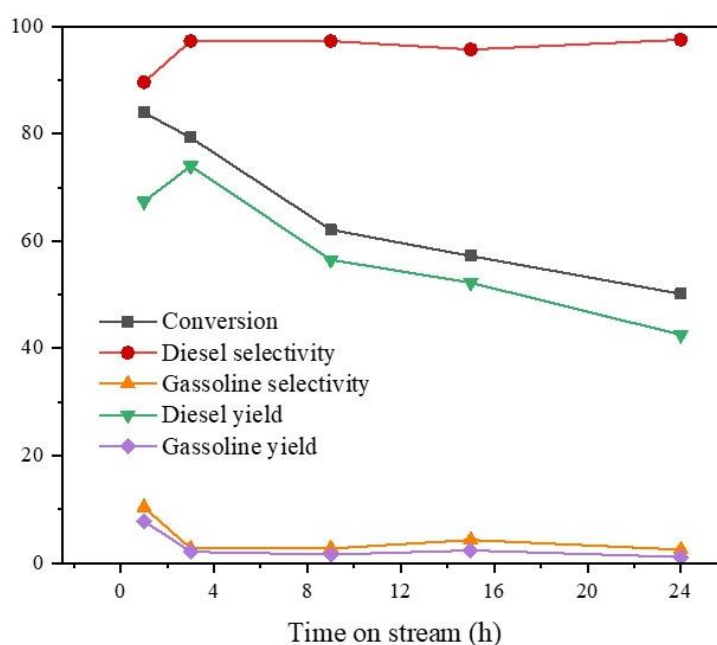
Figure 23 Stability of sulfided NiMo/γ-Al$_2$O$_3$ catalyst under pure carbon monoxide (PFAD feedstock), operating temperature = 330 °C, pressure = 50 bar of pure carbon monoxide, LHSV = 1 h^{-1} and gas/feed ratio = 500 (v/v)).

Table 11 Comparison of palm fatty acid distillate (PFAD) conversion and yields of hydrocarbon fractions (%) over sulfided NiMo catalysts supported on alumina (Operating temperature = 330 °C and LHSV = 1 h^{-1}).

Sample	conversion	<C$_{15}$	n-C$_{15-18}$	>n-C$_{18}$	n-C$_{15-18}$	iso- n-C$_{15-18}$
30 bar of pure hydrogen						
250 v/v	97.0	2.62	97.33	0.06	0.97	0.03
500 v/v	98.89	4.33	95.20	0.48	0.98	0.02
1000 v/v	98.9	3.56	95.49	0.95	0.99	0.01
50 bar of pure hydrogen						
250 v/v	99.43	3.50	96.45	0.06	0.99	0.01
500 v/v	99.32	4.61	94.91	0.48	0.99	0.01
1000 v/v	98.89	3.54	95.84	0.62	0.99	0.01
30 bar of synthesis gas						
250 v/v	99.43	4.14	93.59	2.27	0.90	0.10
500 v/v	99.32	5.43	93.25	1.32	0.97	0.03
1000 v/v	98.89	4.71	93.84	1.45	0.98	0.02
50 bar of synthesis gas						
250 v/v	99.26	8.31	87.23	4.46	0.84	0.16
500 v/v	98.69	4.06	94.74	1.21	0.99	0.01
1000 v/v	99.81	2.81	93.88	3.31	0.95	0.05
50 bar of carbon monoxide						
500 v/v	50.14	62.55	36.65	0.80	0.17	0.83
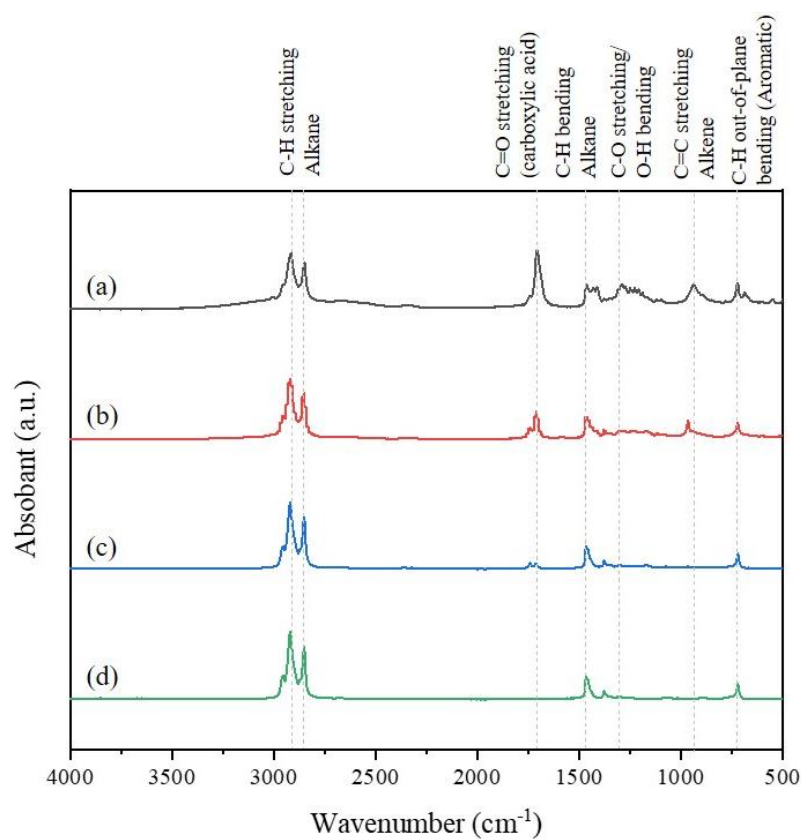
Figure 24 The FTIR spectrums of (a) palm fatty acid distillate (PFAD). The Hydrotreating reaction performed over sulfided NiMo/γ-Al$_2$O$_3$ under pressure of (b) pure carbon monoxide, (c) pure hydrogen, and (d) synthesis gas. (Operating temperature = 330 °C, pressure = 50 bar, gas/feed ratio = 500 (v/v) and LHSV = 1 h^{-1}).

When considering among of coke formation under pure carbon monoxide, pure hydrogen and synthesis gas at the same operating pressure, it found that the hydrotreating under pure carbon monoxide and synthesis gas has more carbon deposition than pure hydrogen (Figure 25). In the case of pure hydrogen, the carbon deposition on the catalyst caused by carbon loss from feedstock via decarbonylation/decarboxylation reaction. Besides, the carbon deposition on catalyst under synthesis gas can occur from carbon monoxide resources. Moreover, at a high temperature of 700 °C to 800 °C and above 850 °C assigned to complex species absorbed on a catalyst [68].
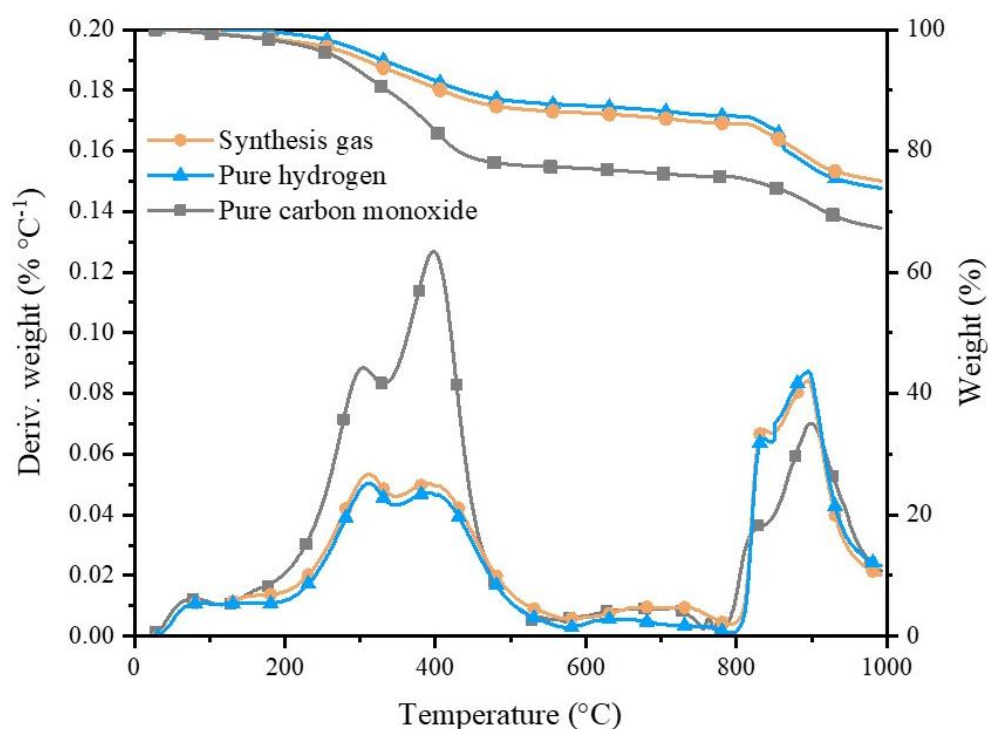
Figure 25 Thermogravimetric analysis of spent NiMo/γ-Al$_2$O$_3$ catalysts. The operating condition at 50 bar of pure carbon monoxide, pure hydrogen and synthesis gas, temperature of 330 °C, LHSV = 1h^{-1}, gas/feed ratio = 500 v/v by PFAD feedstock.
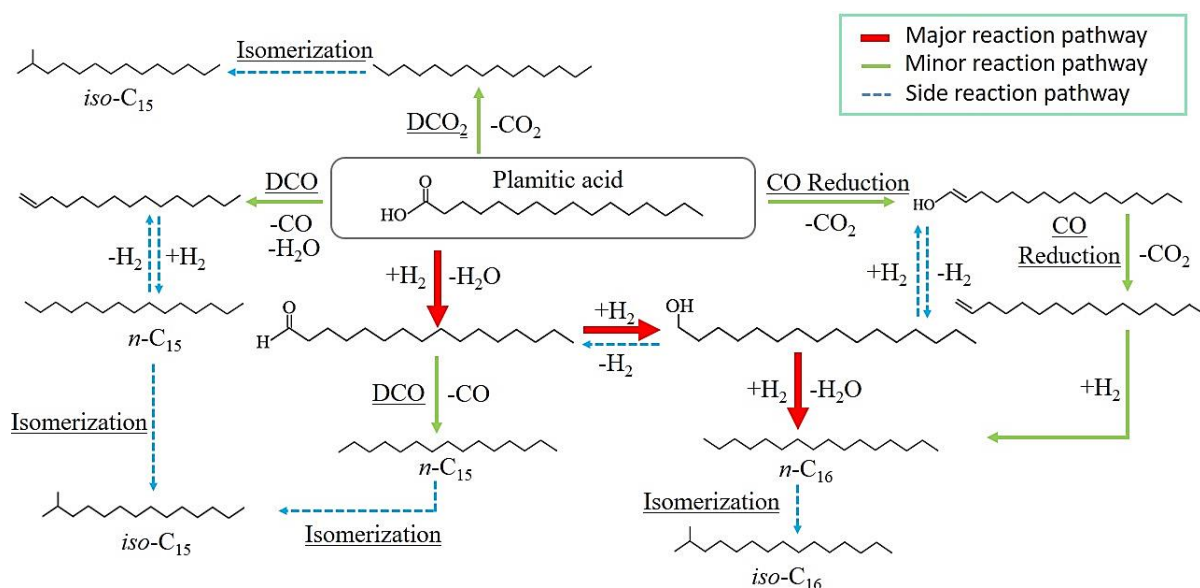
Figure 26 Proposed possible reaction pathways for deoxygenation of PFAD feedstock over a sulfided NiMo/γ-Al$_2$O$_3$ catalyst under synthesis gas.

From liquid product characterization, it can write the proposed possible reaction pathways for deoxygenation of palm fatty acid distillate feedstock over a sulfided NiMo/γ-Al$_2$O$_3$ catalyst under synthesis gas presented in Figure 26. Palmitic acid as a model of palm fatty acid distillate feedstock. In the major reaction pathways, the fatty acid was deoxygenated through hydrodeoxygenation at C-O cleavage and C=O cleavage, respectively. The product partially deoxygenated intermediates are alcohol and aldehyde. Then hydrodeoxygenation to produce n-C$_{16}$ and iso-C$_{16}$ through isomerization. Besides, the minor reaction pathways are decarbonylation and decarboxylation reaction pathways that lose carbon atom into CO and CO$_2$, respectively. However, In the case of pure carbon monoxide show the formation of alkene and iso-C$_{16}$ through CO reduction.

5.2.2 Effect of synthesis gas using on other catalysts

To investigate the catalytic deoxygenation at different catalysts under the operating pressure of the synthesis gas atmosphere. The reaction carried out at an operating temperature of 330 °C, operating pressure at 50 bar of synthesis gas, gas/feed ratio of 500 v/v and LHSV = 1 h^{-1}. The conversion of palm fatty acid distillate over three hydrotreating catalysts i.e. sulfided NiMo/γ-Al$_2$O$_3$, reduced NiMo/γ-Al$_2$O$_3$, and reduced NiCu/HZSM-5 catalyst and shown in Figure 27. The result indicated that the highest conversion is sulfided NiMo/γ-Al$_2$O$_3$ (approximately 100%) and still stable to 42 h. On the other hand, the reduced NiMo/γ-Al$_2$O$_3$ and NiCu/HZSM-5 have lower conversion than sulfide NiMo/γ-Al$_2$O$_3$ catalyst. Initially, the conversion over the reduced NiMo/γ-Al$_2$O$_3$ catalyst is 85.4% and decreases to 73% while the conversion over NiCu/HZSM-5 catalyst is 97% and drops to 78%. Interestingly, the catalytic deoxygenation can operate under the operating pressure of synthesis gas over three conventional catalysts and not deactivated in 42 h. To confirm the GC result, the functional group of liquid products identifies by FTIR analysis shown in Figure 34. It was found that a fatty acid peak over reduced NiMo/γ-Al$_2$O$_3$ and reduced the NiCu/HZSM-5 catalyst. Moreover, this result shows the peak of alkane lowest in NiCu/HZSM-5 catalyst. In the case of NiCu/HZSM-5 catalyst compared with 40 bar of pure hydrogen (Figure 35), it indicating that the use of synthesis gas over cracking NiCu/HZSM-5 catalyst work as good as pure hydrogen in term of feedstock conversion.

The selectivity and yield of the hydrotreated catalyst were shown in Figure 28. The result shown that the diesel selectivity and diesel yield decrease in order sulfided NiMo/γ-Al$_2$O$_3$ > reduced NiMo/γ-Al$_2$O$_3$ > reduced NiCu/HZSM-5. It is observed that the highest diesel yield at 78% of sulfided NiMo/γ-Al$_2$O$_3$. However, the solid acid catalyst or cracking catalyst i.e. NiCu/HZSM-5 showed a high percentage of gasoline yield (65%) and diesel yield (18.4%) because the HZSM-5 support catalyst has a strong acid site [2].

Figure 29 shows the gaseous composition product, the products of NiMo/γ-Al$_2$O$_3$ are CO, CH$_4$, and low content of CO$_2$. The gas product from NiCu/HZSM-5 mainly CO, which excess from the reaction. Moreover, the CO in gaseous products refers to atom carbon loss from the cracking reaction of feedstock. Besides, the CO can refer to the DCO reaction pathway.
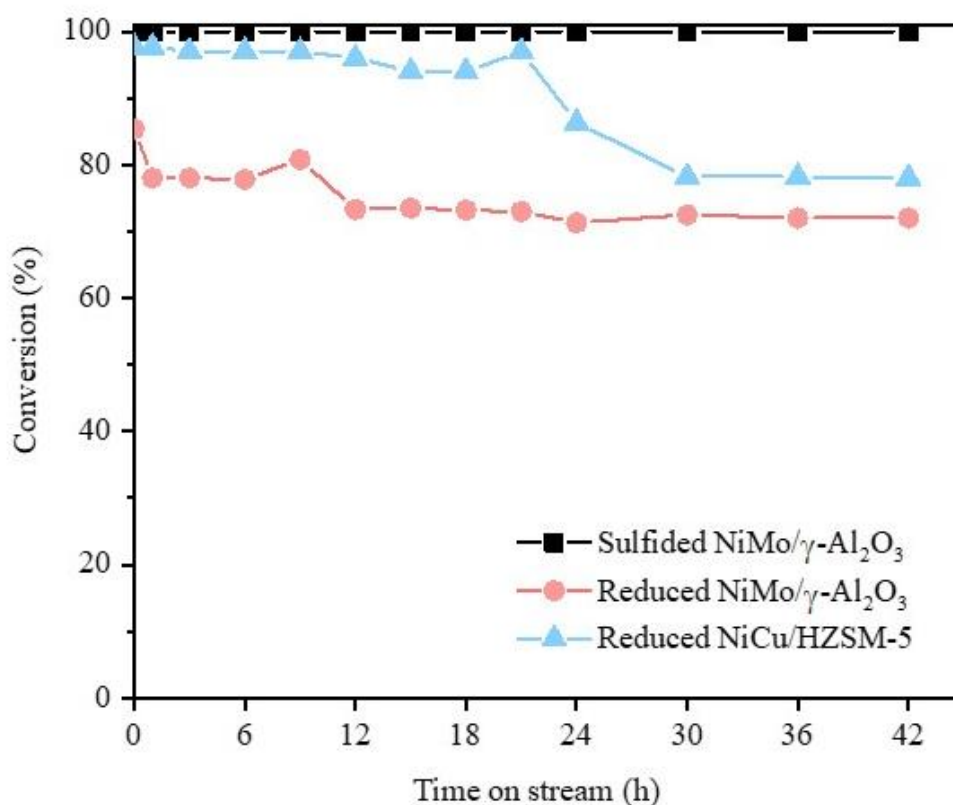
Figure 27 The conversion of sulfided NiMo/γ-Al$_2$O$_3$, reduced NiMo/γ-Al$_2$O$_3$ and reduced NiCu/HZSM-5 catalyst. The reactions were performed by by PFAD feedstock under operating pressure at 50 bar of synthesis gas, gas/feed ratio of 500 v/v and liquid hour space velocity (LHSV) = 1 h^{-1}.
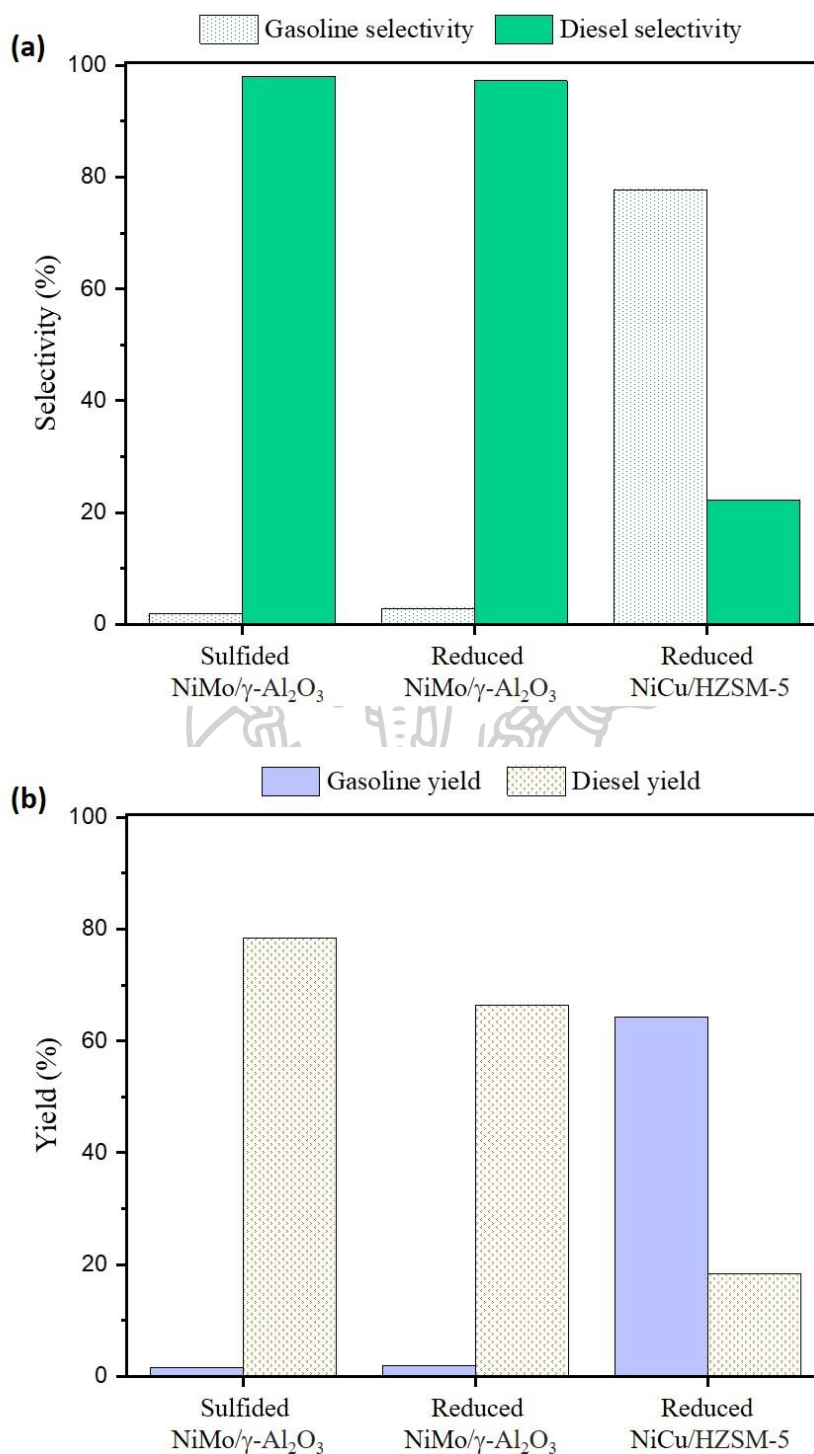
Figure 28 The (a) selectivity and (b) yield of gasoline and diesel over sulfided NiMo/γ-Al$_2$O$_3$, reduced NiMo/γ-Al$_2$O$_3$ and reduced NiCu/HZSM-5 catalyst. The reactions were performed by PFAD feedstock under operating pressure at 50 bar of synthesis gas, gas/feed ratio of 500 v/v and liquid hour space velocity (LHSV) = 1 h^{-1}.

Figure 29 The mole fraction of gasous products over sulfided NiMo/γ-Al$_2$O$_3$, reduced NiMo/γ-Al$_2$O$_3$ and reduced NiCu/HZSM-5 catalyst. The reactions were performed by PFAD feedstock under operating pressure at 50 bar of synthesis gas, gas/feed ratio of 500 v/v and liquid hour space velocity (LHSV) = 1 h^{-1}.

The liquid hydrocarbons distribution of sulfided NiMo/γ-Al$_2$O$_3$, reduced NiMo/γ-Al$_2$O$_3$ and reduced NiCu/HZSM-5 catalysts shown in Figure 30, 31 and 32, respectively. In the case of sulfided NiMo/γ-Al$_2$O$_3$ catalyst and reduced NiMo/γ-Al$_2$O$_3$ catalyst, it favored the hydrodeoxygenation as a major reaction pathway resulting in the liquid hydrocarbons consisted mostly of n-C$_{16}$ and n-C$_{18}$. The similar behavior of both catalysts due to the same acid sites of the alumina support [32]. The NiCu/HZSM-5 cracking catalyst shows a high percentage of light hydrocarbon (n-C$_5$-n-C$_{11}$) that in range of gasoline so high of gasoline selectivity and gasoline yield. In the case of the NiCu/HZSM-5 catalyst, the results show the liquid product is mainly light hydrocarbon because of the microspore of the HZSM-5 catalyst that a small channels. Moreover, the light hydrocarbon produced from the secondary cracking during the catalytic cracking process [69, 70]. The microspore catalysts are a small

channel and a long diffusion path for feedstock [57]. Moreover, microporous HZSM-5 supports can provide more cracking sites for gasoline production than mesoporous γ-Al_2O_3. Therefore, the pore structure of the catalyst will cause more secondary cracking and affected low diesel selectivity.

Table 12 shows the composition of the liquid product from the catalytic deoxygenation of palm fatty acid distillate over the different catalysts. It found that the most fraction of sulfided NiMo/γ-Al_2O_3 and reduced NiMo/γ-Al_2O_3 catalysts are n-C_{15}-n-C_{18} and some the amount of heavy molecule that higher than n-C_{18}. The formation of heavy hydrocarbon can be formed by oligomerization reactions [32].

The hydrocarbon product distribution via the hydrotreating process under the operating pressure of the synthesis gas atmosphere shown in the chromatograms of palm fatty acid distillate feedstock and liquid product by sulfide NiMo/γ-Al_2O_3 and NiCu/HZSM-5 catalyst (see in Figure 33) shown the main component in palm fatty acid distillate consist of palmitic acid and oleic acid that corresponding to fatty acid composition (Table 4). The liquid hydrocarbon of all catalysts in the same operating condition can completely convert to hydrocarbon. The chromatograms from the GC-FID result of sulfide NiMo/γ-Al_2O_3 similar to reduced NiMo/γ-Al_2O_3 (not show) catalysts. Moreover, the light hydrocarbon was significantly in the NiCu/HZSM-5 catalyst. Therefore, the synthesis gas can be used in the hydrotreating process and not affect cracking catalyst ability.
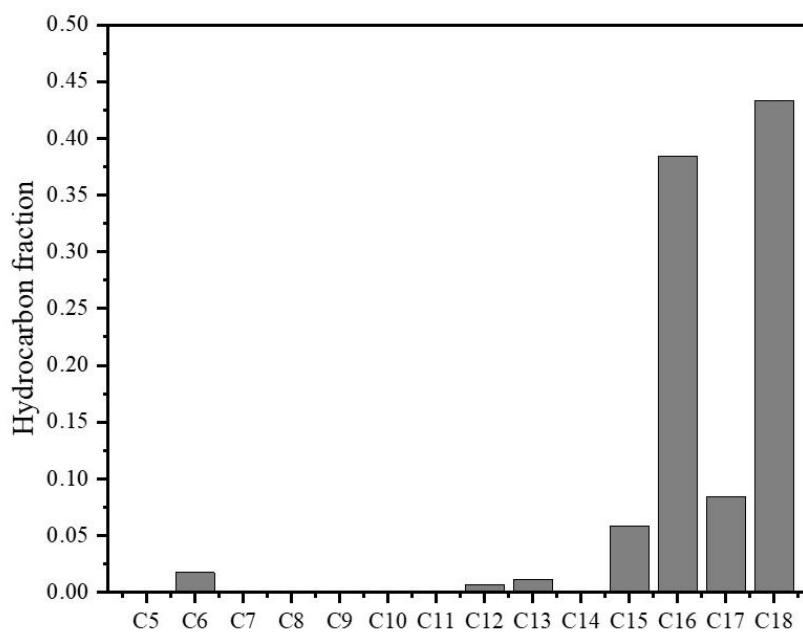
Figure 30 The liquid product distribution of sulfided NiMo/γ-Al$_2$O$_3$catalyst. The reactions were performed by palm fatty acid distillate (PFAD) feedstock under operating pressure at 50 bar of synthesis gas, gas/feed raatio of 500 v/v and liquid hour space velocity (LHSV) = 1 h^{-1}.
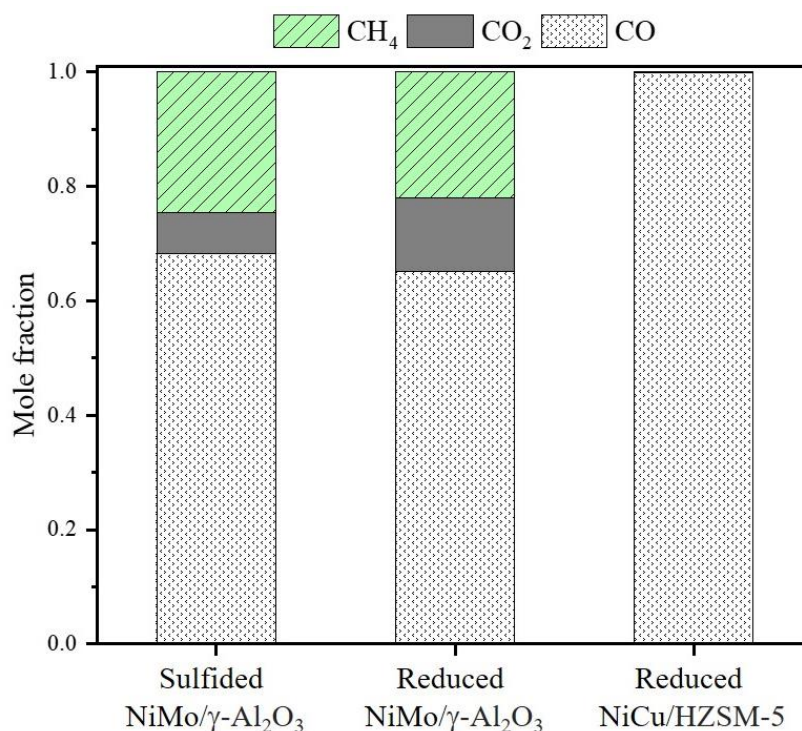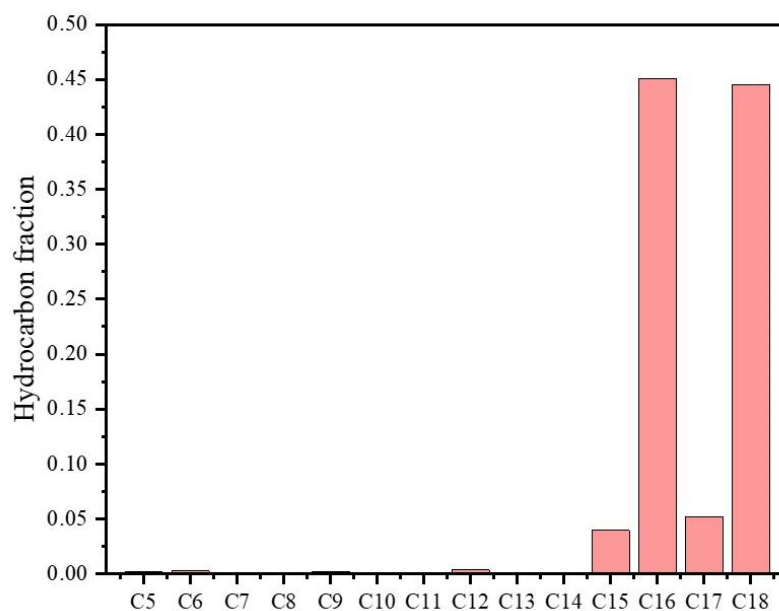

Figure 31 The liquid product distribution of reduced NiMo/γ-Al$_2$O$_3$ catalyst. The reactions were performed by palm fatty acid distillate (PFAD) feedstock under operating pressure at 50 bar of synthesis gas, gas/feed raatio of 500 v/v and liquid hour space velocity (LHSV) = 1 h^{-1}.
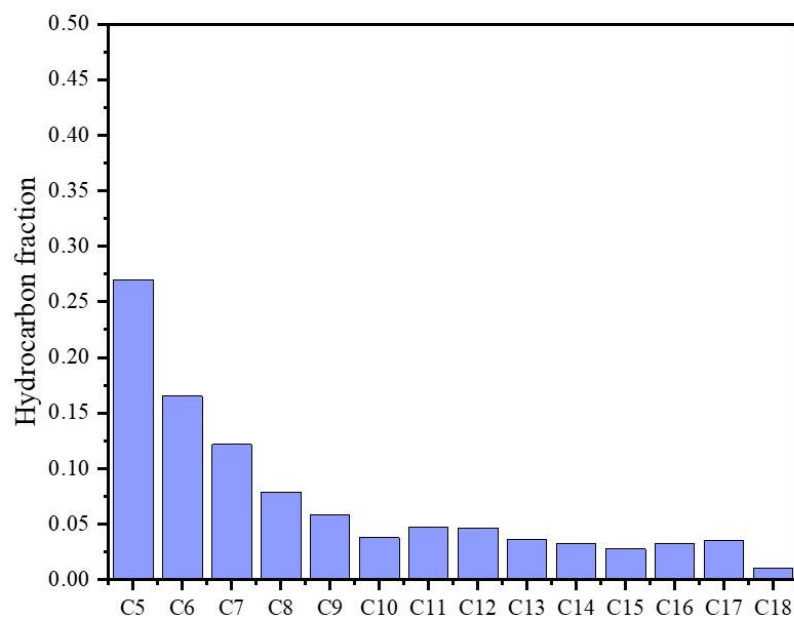
Figure 32 The liquid product distribution of reduced NiCu/HZSM-5 catalyst. The reactions were performed by palm fatty acid distillate (PFAD) feedstock under operating pressure at 50 bar of synthesis gas, gas/feed raatio of 500 v/v and liquid hour space velocity (LHSV) = 1 h^{-1}.

Table 12 Composition of the liquid product from the catalytic deoxygenation of palm fatty acid distillate (PFAD) feedstock over the different catalysts.

Catalysts	Liquid product composition (%)					
	$<n\text{-}C_{15}$	$n\text{-}C_{15}$	$n\text{-}C_{16}$	$n\text{-}C_{17}$	$n\text{-}C_{18}$	$>n\text{-}C_{18}$
Sulfide NiMo/γ-Al$_2$O$_3$	4.06	5.76	37.97	8.34	42.73	1.21
Reduced NiMo/γ-Al$_2$O$_3$	4.51	3.70	42.03	4.84	41.52	3.40
Reduced NiCu/HZSM-5	78.68	4.18	6.46	6.31	4.36	0.02
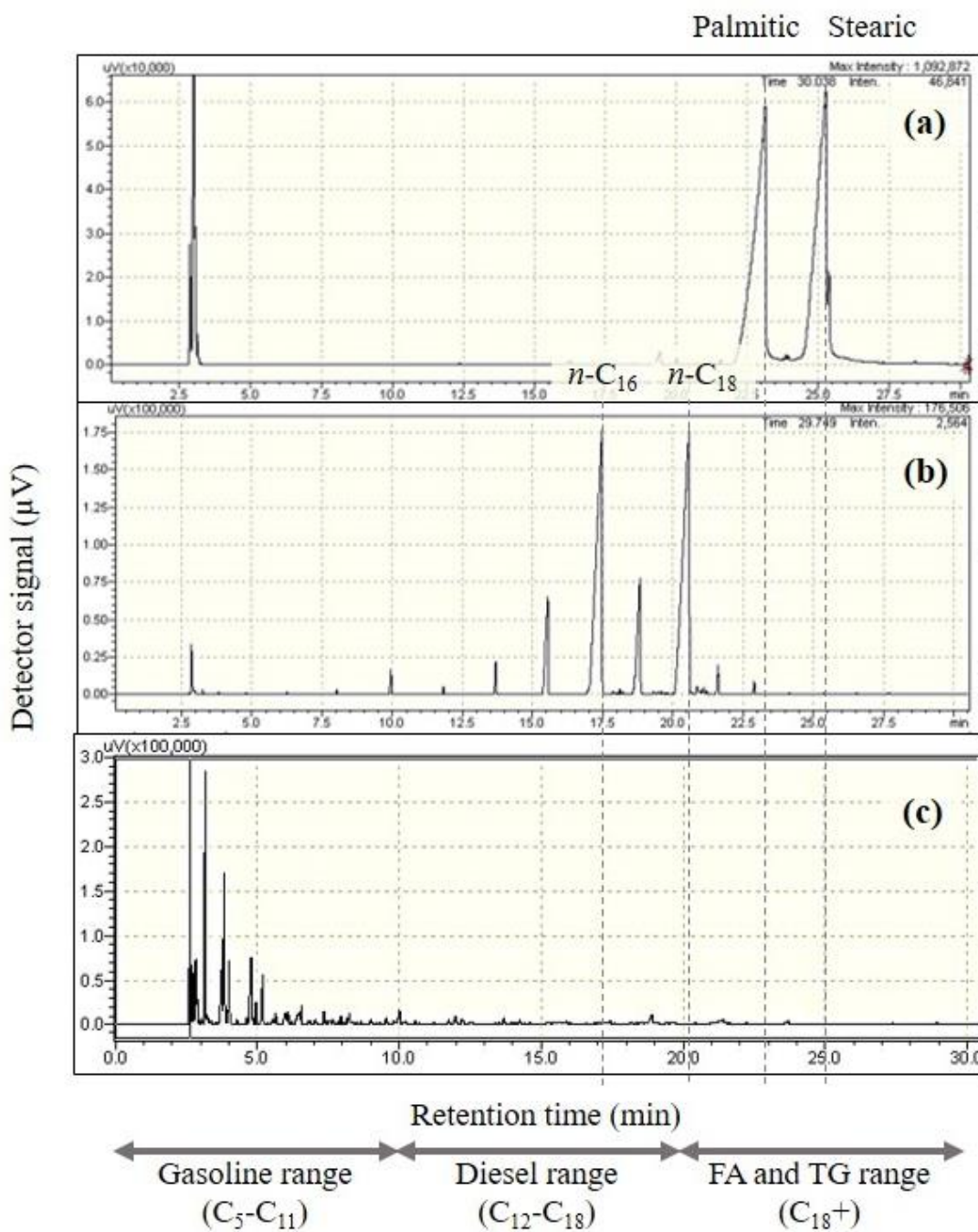
Figure 33 Chromatograms of (a) palm fatty acid distillate (PFAD) feedstock, (b) hydrotreated product of sulfided NiMo/γ-Al$_2$O$_3$ catalyst and (c) hydrotreated product of reduced NiCu/HZSM-5 catalyst. The reactions were performed at operating temperature = 330 °C, operating pressure = 50 bar, synthesis gas/feed ratio = 500 v/v and liquid hour space velocity (LHSV) = 1 h^{-1}.
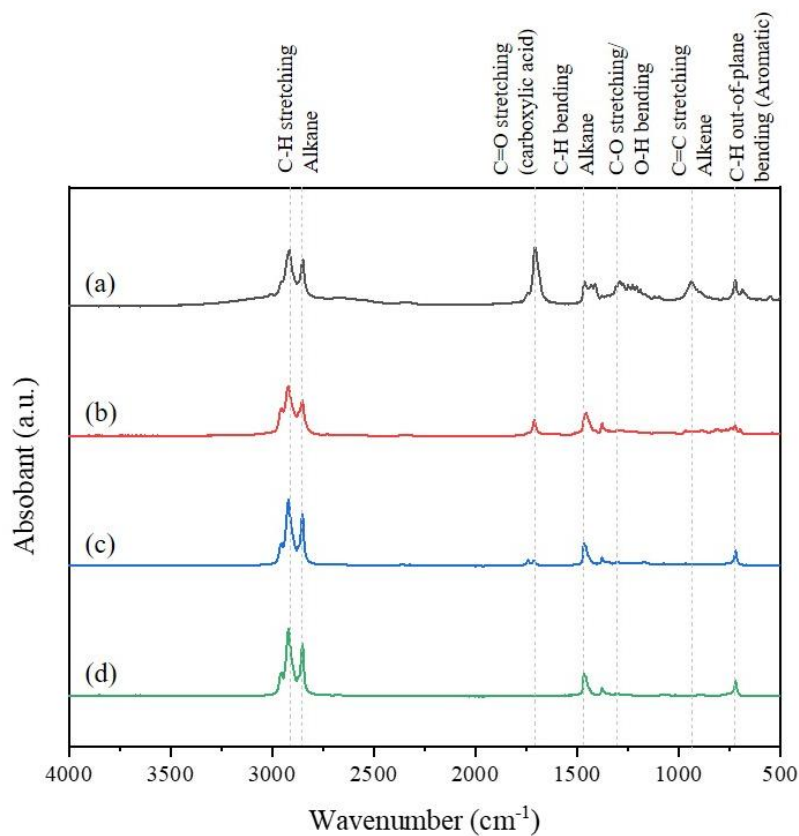
Figure 34 The FT-IR spectrums of (a) palm fatty acid distillate (PFAD) feedstock. The hydrotreating reaction performed over (b) reduced NiCu/HZSM-5, (c) reduced NiMo/γ-Al$_2$O$_3$ and (d) sulfided NiMo/γ-Al$_2$O$_3$. (Operating temperature = 330 °C, pressure = 50 bar of synthesis gas, LHSV = 1 h^{-1} and gas/feed ratio = 500 (v/v)).
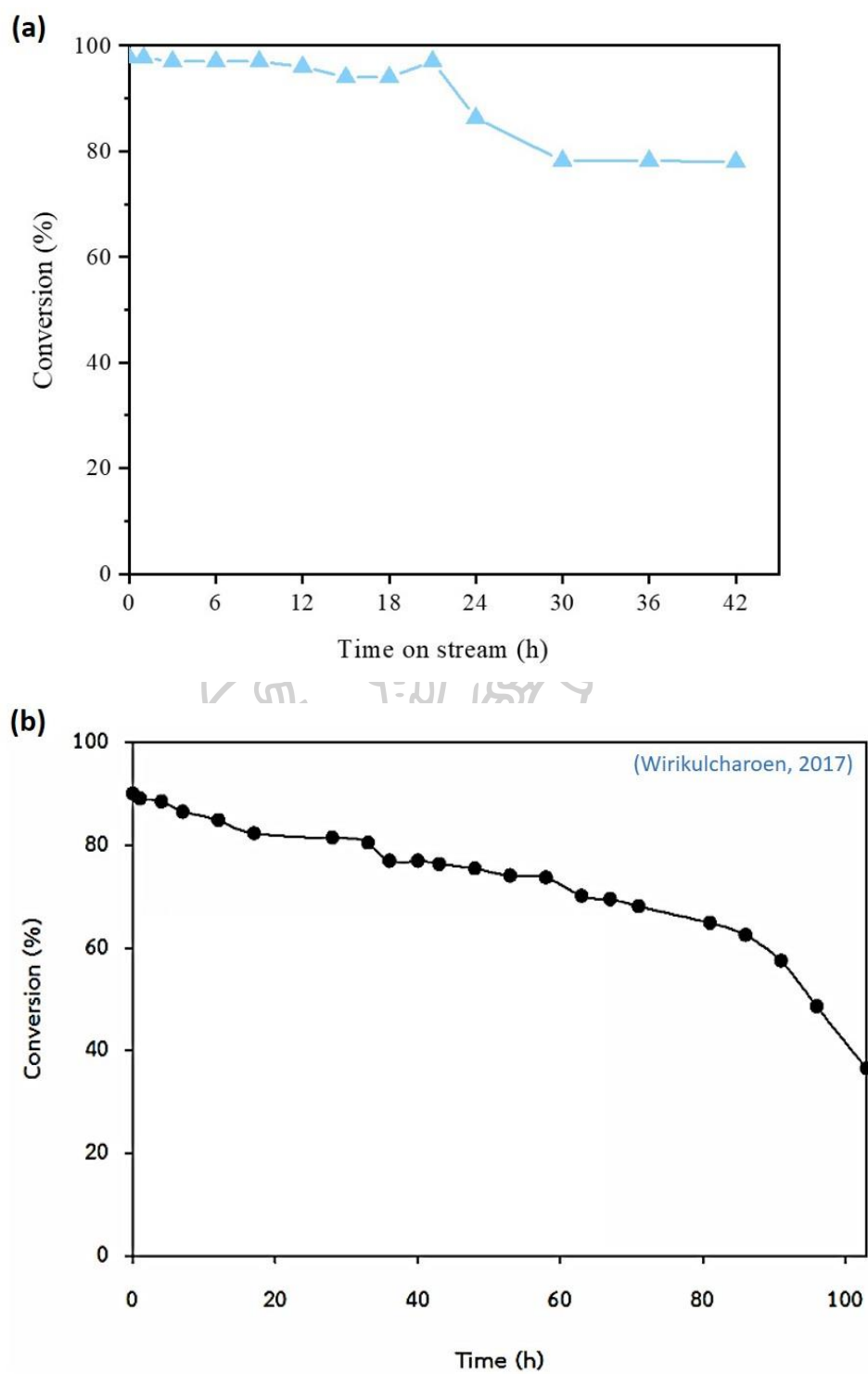
Figure 35 Catalyst stability test over 12.5%Ni2.5%Cu/HZSM-5 cracking catalyst under (a) synthesis gas and (b) pure hydrogen [26].

CHAPTER VI

CONCLUSION

6.1 Conclusion

The green diesel production via catalytic deoxygenation under continuous process using palm fatty acid distillate (PFAD) as feedstock. The reaction performed under an operating temperature of 330 °C and a liquid hour space velocity of 1 h^{-1}. To estimate the performance of synthesis gas instead of pure hydrogen by varied operating pressure and gas/feed ratio, the results show that synthesis gas can give performance similar to pure hydrogen. The hydrodeoxygenation as a dominant reaction pathway for sulfided NiMo/γ-Al$_2$O$_3$ catalyst. The reaction pathways are also found to be not different under pure hydrogen and synthesis gas. The containing of CO in the synthesis gas could promote the reaction through the CO reduction, therefore the amount of carbon in the liquid product from synthesis gas higher than pure hydrogen gas. In operating pressure of pure carbon monoxide, the conversion of PFAD at 85% and dramatically dropped to 50% within 24 h of operating. Although, the hydrotreating process over sulfided NiMo/γ-Al$_2$O$_3$ catalyst cannot operate under pure carbon monoxide but show the formation of alkene and isomerization reaction though CO reduction. However, the hydrogen still significantly for sulfided NiMo/γ-Al$_2$O$_3$ catalyst to prevent the deactivation catalyst. Moreover, the synthesis gas can operate with reduced NiMo/γ-Al$_2$O$_3$ and cracking NiCu/HZSM-5 catalyst without deactivation in 42 h. Besides, the activity of the NiCu/HZSM-5 cracking catalyst under synthesis gas works as good as pure hydrogen.

REFERENCES

1.   Wang, C., et al., *One-Step Hydrotreatment of Vegetable Oil to Produce High Quality Diesel-Range Alkanes.* ChemSusChem, 2012. **5**(10): p. 1974-1983.
2.   Liu, Y., et al., *Hydrotreatment of vegetable oils to produce bio-hydrogenated diesel and liquefied petroleum gas fuel over catalysts containing sulfided Ni–Mo and solid acids.* Energy & Fuels, 2011. **25**(10): p. 4675-4685.
3.   Kubička, D., et al., *Effect of support-active phase interactions on the catalyst activity and selectivity in deoxygenation of triglycerides.* Applied Catalysis B: Environmental, 2014. **145**: p. 101-107.
4.   Chen, N., et al., *Effects of Si/Al ratio and Pt loading on Pt/SAPO-11 catalysts in hydroconversion of Jatropha oil.* Applied Catalysis A: General, 2013. **466**: p. 105-115.
5.   Kubičková, I., et al., *Hydrocarbons for diesel fuel via decarboxylation of vegetable oils.* Catalysis Today, 2005. **106**(1-4): p. 197-200.
6.   Immer, J.G. and H.H. Lamb, *Fed-batch catalytic deoxygenation of free fatty acids.* Energy & fuels, 2010. **24**(10): p. 5291-5299.
7.   Madsen, A.T., et al., *Step changes and deactivation behavior in the continuous decarboxylation of stearic acid.* Industrial & engineering chemistry research, 2011. **50**(19): p. 11049-11058.
8.   Immer, J.G., M.J. Kelly, and H.H. Lamb, *Catalytic reaction pathways in liquid-phase deoxygenation of C18 free fatty acids.* Applied Catalysis A: General, 2010. **375**(1): p. 134-139.
9.   Yang, X., et al., *Characterization and performance evaluation of Ni-based catalysts with Ce promoter for methane and hydrocarbons steam reforming process.* Fuel, 2016. **179**: p. 353-361.
10.   Angeli, S.D., et al., *Catalyst development for steam reforming of methane and model biogas at low temperature.* Applied Catalysis B: Environmental, 2016. **181**: p. 34-46.
11.   Tanneru, S.K. and P.H. Steele, *Production of liquid hydrocarbons from pretreated bio-oil via catalytic deoxygenation with syngas.* Renewable Energy, 2015. **80**: p. 251-258.
12.   Pongsiriyakul, K., et al., *Alternative Hydrocarbon Biofuel Production via Hydrotreating under a Synthesis Gas Atmosphere.* Energy & Fuels, 2017. **31**(11): p. 12256-12262.
13.   Kubička, D. and L. Kaluža, *Deoxygenation of vegetable oils over sulfided Ni, Mo and NiMo catalysts.* Applied Catalysis A: General, 2010. **372**(2): p. 199-208.
14.   Huber, G.W., P. O'Connor, and A. Corma, *Processing biomass in conventional oil refineries: Production of high quality diesel by hydrotreating vegetable oils in heavy vacuum oil mixtures.* Applied Catalysis A: General, 2007. **329**: p. 120-129.
15.   Srifa, A., et al., *Production of bio-hydrogenated diesel by catalytic hydrotreating of palm oil over NiMoS2/γ-Al2O3 catalyst.* Bioresource technology, 2014. **158**: p. 81-90.
16.   Kim, T.-H., et al., *Effects of fatty acid compositions on heavy oligomer formation and catalyst deactivation during deoxygenation of triglycerides.* ACS Sustainable Chemistry & Engineering, 2018. **6**(12): p. 17168-17177.

17. Srifa, A., et al., *Roles of monometallic catalysts in hydrodeoxygenation of palm oil to green diesel.* Chemical Engineering Journal, 2015. **278**: p. 249-258.

18. Nimkarde, M.R. and P.D. Vaidya, *Toward diesel production from karanja oil hydrotreating over CoMo and NiMo catalysts.* Energy & Fuels, 2016. **30**(4): p. 3107-3112.

19. Thongkumkoon, S., et al., *Catalytic activity of trimetallic sulfided Re-Ni-Mo/γ-Al2O3 toward deoxygenation of palm feedstocks.* Renewable Energy, 2019. **140**: p. 111-123.

20. Itthibenchapong, V., et al., *Deoxygenation of palm kernel oil to jet fuel-like hydrocarbons using Ni-MoS2/γ-Al2O3 catalysts.* Energy conversion and management, 2017. **134**: p. 188-196.

21. Kim, S.K., et al., *Production of renewable diesel via catalytic deoxygenation of natural triglycerides: Comprehensive understanding of reaction intermediates and hydrocarbons.* Applied energy, 2014. **116**: p. 199-205.

22. Ala'a, H., et al., *Efficient utilization of waste date pits for the synthesis of green diesel and jet fuel fractions.* Energy Conversion and Management, 2016. **127**: p. 226-232.

23. Sotelo-Boyás, R., Y. Liu, and T. Minowa, *Renewable diesel production from the hydrotreating of rapeseed oil with Pt/Zeolite and NiMo/Al2O3 catalysts.* Industrial & Engineering Chemistry Research, 2011. **50**(5): p. 2791-2799.

24. Veriansyah, B., et al., *Production of renewable diesel by hydroprocessing of soybean oil: Effect of catalysts.* Fuel, 2012. **94**: p. 578-585.

25. Kaewmeesri, R., et al., *Deoxygenation of waste chicken fats to green diesel over Ni/Al2O3: effect of water and free fatty acid content.* Energy & Fuels, 2015. **29**(2): p. 833-840.

26. Wirikulcharoen, P., *CONTINUOUS HYDROTREATING PROCESS OF PALM FATTY ACID DISTILLATE (PFAD) OVER BIMETALLIC NiCu/HZSM-5 CATALYST FOR BIO JET FUEL PRODUCTION.* 2017, Chulalongkorn University.

27. Srifa, A., et al., *Catalytic behaviors of Ni/γ-Al 2 O 3 and Co/γ-Al 2 O 3 during the hydrodeoxygenation of palm oil.* Catalysis Science & Technology, 2015. **5**(7): p. 3693-3705.

28. Monnier, J., et al., *Hydrodeoxygenation of oleic acid and canola oil over alumina-supported metal nitrides.* Applied Catalysis A: General, 2010. **382**(2): p. 176-180.

29. Wang, F., et al., *Activated carbon supported molybdenum and tungsten carbides for hydrotreatment of fatty acids into green diesel.* Fuel, 2018. **228**: p. 103-111.

30. Liu, J., et al., *Hydroprocessing of Jatropha oil over NiMoCe/Al2O3 catalyst.* International journal of hydrogen energy, 2012. **37**(23): p. 17731-17737.

31. Krár, M., et al., *Fuel purpose hydrotreating of sunflower oil on CoMo/Al2O3 catalyst.* Bioresource technology, 2010. **101**(23): p. 9287-9293.

32. Taromi, A.A. and S. Kaliaguine, *Green diesel production via continuous hydrotreatment of triglycerides over mesostructured γ-alumina supported NiMo/CoMo catalysts.* Fuel processing technology, 2018. **171**: p. 20-30.

33. Patil, S.J. and P.D. Vaidya, *Production of hydrotreated jatropha oil using Co–Mo and Ni–Mo catalysts and its blending with petroleum diesel.* Energy & Fuels, 2018. **32**(2): p. 1812-1821.

34. Gong, S., A. Shinozaki, and E.W. Qian, *Role of support in hydrotreatment of jatropha oil over sulfided NiMo catalysts.* Industrial & engineering chemistry research, 2012. **51**(43): p. 13953-13960.

35. Kovács, S., et al., *Fuel production by hydrotreating of triglycerides on NiMo/Al2O3/F catalyst.* Chemical Engineering Journal, 2011. **176**: p. 237-243.

36. Ameen, M., et al., *Catalytic hydrodeoxygenation of rubber seed oil over sonochemically synthesized Ni-Mo/γ-Al2O3 catalyst for green diesel production.* Ultrasonics Sonochemistry, 2019. **51**: p. 90-102.

37. Kim, S.K., et al., *Mo2C/graphene nanocomposite as a hydrodeoxygenation catalyst for the production of diesel range hydrocarbons.* Acs Catalysis, 2015. **5**(6): p. 3292-3303.

38. Manchanda, T., R. Tyagi, and D.K. Sharma, *Comparison of fuel characteristics of green (renewable) diesel with biodiesel obtainable from algal oil and vegetable oil.* Energy Sources, Part A: Recovery, Utilization, and Environmental Effects, 2018. **40**(1): p. 54-59.

39. Mikulec, J., et al., *Second generation diesel fuel from renewable sources.* Journal of Cleaner Production, 2010. **18**(9): p. 917-926.

40. Zhao, C., T. Brück, and J.A. Lercher, *Catalytic deoxygenation of microalgae oil to green hydrocarbons.* Green Chemistry, 2013. **15**(7): p. 1720-1739.

41. Gosselink, R.W., et al., *Reaction pathways for the deoxygenation of vegetable oils and related model compounds.* ChemSusChem, 2013. **6**(9): p. 1576-1594.

42. Kiatkittipong, W., et al., *Diesel-like hydrocarbon production from hydroprocessing of relevant refining palm oil.* Fuel processing technology, 2013. **116**: p. 16-26.

43. Krokidis, X., et al., *Theoretical study of the dehydration process of boehmite to γ-alumina.* The Journal of Physical Chemistry B, 2001. **105**(22): p. 5121-5130.

44. Sifontes, Á.B., et al., *Preparation of functionalized porous nano-γ-Al2O3 powders employing colophony extract.* Biotechnology Reports, 2014. **4**: p. 21-29.

45. Wang, Z., et al., *Synthesis and characterization of amorphous Al2O3 and γ-Al2O3 by spray pyrolysis.* Green Processing and Synthesis, 2016. **5**(3): p. 305-310.

46. Sifontes, A., et al., *Preparation of γ-alumina foams of high surface area employing the polyurethane sponge replica method.* Latin American applied research, 2010. **40**(2): p. 185.

47. Palcheva, R., et al., *NiMo/γ-Al2O3 catalysts from ni heteropolyoxomolybdate and effect of alumina modification by b, co, or ni.* Chinese Journal of Catalysis, 2012. **33**(4-6): p. 952-961.

48. Shelke, P.D. and A.S. Rajbhoj, *Electrochemical synthesis and their photocatalytic application of mesoporous γ-Al2O3 nanoparticles.* Der Chemica Sinica, 2017. **8**: p. 482-6.

49. Leyva, C., M.S. Rana, and J. Ancheyta, *Surface characterization of Al2O3–SiO2 supported NiMo catalysts: An effect of support composition.* Catalysis Today, 2008. **130**(2-4): p. 345-353.

50. Liu, F., et al., *A comparison of NiMo/Al2O3 catalysts prepared by impregnation and coprecipitation methods for hydrodesulfurization of dibenzothiophene.* The Journal of Physical Chemistry C, 2007. **111**(20): p. 7396-7402.

51. Veeramalai, C.P., et al., *Enhanced field emission properties of molybdenum disulphide few layer nanosheets synthesized by hydrothermal method.* Applied Surface Science, 2016. **389**: p. 1017-1022.

52. Yin, C., et al., *A novel porous ammonium nickel molybdate as the catalyst precursor towards deep hydrodesulfurization of gas oil.* Fuel, 2013. **107**: p. 873-878.

53. Zhu, X., et al., *Synthesis of nano-TiO 2-decorated MoS 2 nanosheets for lithium ion batteries.* New Journal of Chemistry, 2015. **39**(1): p. 683-688.

54. Wang, Y., H. Lin, and Y. Zheng, *Hydrotreatment of lignocellulosic biomass derived oil using a sulfided NiMo/γ-Al 2 O 3 catalyst.* Catalysis Science & Technology, 2014. **4**(1): p. 109-119.

55. Corma, A., *From microporous to mesoporous molecular sieve materials and their use in catalysis.* Chemical reviews, 1997. **97**(6): p. 2373-2420.

56. Xu, Y., et al., *Methane activation without using oxidants over Mo/HZSM-5 zeolite catalysts.* Catalysis letters, 1994. **30**(1-4): p. 135-149.

57. Wang, H., et al., *Support effects on hydrotreating of soybean oil over NiMo carbide catalyst.* Fuel, 2013. **111**: p. 81-87.

58. AKASSUPHA, B. and W. Kiatkitipong, *Aviation fuel production from renewable feedstock by a single-step hydrotreating process.* 2018, Silpakorn University.

59. Yakovlev, V., et al., *Development of new catalytic systems for upgraded bio-fuels production from bio-crude-oil and biodiesel.* Catalysis Today, 2009. **144**(3-4): p. 362-366.

60. Horiguchi, J., et al., *Mesoporous NiO–Al2O3 catalyst for high pressure partial oxidation of methane to syngas.* Applied Catalysis A: General, 2011. **392**(1-2): p. 86-92.

61. Guo, Q., et al., *Catalytic hydrodeoxygenation of algae bio-oil over bimetallic Ni–Cu/ZrO2 catalysts.* Industrial & engineering chemistry research, 2015. **54**(3): p. 890-899.

62. Tran, N.T., et al., *Vapor-phase hydrodeoxygenation of guaiacol on Al-MCM-41 supported Ni and Co catalysts.* Applied Catalysis A: General, 2016. **512**: p. 93-100.

63. Bkour, Q., et al., *A highly active and stable bimetallic Ni-Mo2C catalyst for a partial oxidation of jet fuel.* Applied Catalysis B: Environmental, 2019. **245**: p. 613-622.

64. Peña, A.G., et al., *Fourier transform infrared-attenuated total reflectance (FTIR-ATR) spectroscopy and chemometric techniques for the determination of adulteration in petrodiesel/biodiesel blends.* Química Nova, 2014. **37**(3): p. 392-397.

65. Che Man, Y., et al., *A Fourier transform infrared spectroscopy method for analysis of palm oil adulterated with lard in pre-fried French fries.* International Journal of Food Properties, 2014. **17**(2): p. 354-362.

66. Toba, M., et al., *Hydrodeoxygenation of waste vegetable oil over sulfide catalysts.* Catalysis Today, 2011. **164**(1): p. 533-537.

67. Li, Y., et al., *Coke deposition on Ni/HZSM-5 in bio-oil hydrodeoxygenation processing.* Energy & Fuels, 2015. **29**(3): p. 1722-1728.

68. Boullosa-Eiras, S., et al., *Catalytic hydrodeoxygenation (HDO) of phenol over*

supported molybdenum carbide, nitride, phosphide and oxide catalysts. Catalysis today, 2014. **223**: p. 44-53.

69. Leng, T.Y., A.R. Mohamed, and S. Bhatia, *Catalytic conversion of palm oil to fuels and chemicals.* The Canadian Journal of Chemical Engineering, 1999. **77**(1): p. 156-162.

70. Kubička, D., P. Šimáček, and N. Žilková, *Transformation of vegetable oils into hydrocarbons over mesoporous-alumina-supported CoMo catalysts.* Topics in Catalysis, 2009. **52**(1-2): p. 161-168.

APPENDIX A

Table A.1 Components of *n*-C$_5$ to *n*-C$_{44}$ alkanes in calibration mixture. (Songphon 2011).

Elution order	Compound	CAS#	Percent Purity	Concentration (wt.%)
1	*n*-Pentane (C$_5$)	109-66-0	99%	0.9995 wt./wt.%
2	*n*-Hexane (C$_6$)	110-54-3	99%	0.9995 wt./wt.%
3	*n*-Heptane (C$_7$)	142-82-5	99%	0.9995 wt./wt.%
4	*n*-Octane (C$_8$)	111-65-9	99%	0.9995 wt./wt.%
5	*n*-Nonane (C$_9$)	111-84-2	99%	0.9995 wt./wt.%
6	*n*-Decane (C$_{10}$)	124-18-5	99%	0.9995 wt./wt.%
7	*n*-Undecane (C$_{11}$)	1120-21-4	99%	0.9995 wt./wt.%
8	*n*-Dodecane (C$_{12}$)	112-40-3	99%	0.9995 wt./wt.%
9	*n*-Tetradecane (C$_{14}$)	629-59-4	99%	0.9995 wt./wt.%
10	*n*-Pentadecane (C$_{15}$)	629-62-9	99%	0.9995 wt./wt.%
11	*n*-Hexadecane (C$_{16}$)	544-76-3	99%	0.9995 wt./wt.%
12	*n*-Heptadecane (C$_{17}$)	629-78-7	99%	0.9995 wt./wt.%
13	*n*-Octadecane (C$_{18}$)	593-45-3	99%	0.9995 wt./wt.%
14	*n*-Eicosane (C$_{20}$)	112-95-8	99%	0.9995 wt./wt.%
15	*n*-Tetracosane (C$_{24}$)	646-31-1	99%	0.9995 wt./wt.%
16	*n*-Octacosane (C$_{28}$)	630-02-4	99%	0.9995 wt./wt.%
17	*n*-Dotriacontane (C$_{32}$)	544-85-4	98%	0.9991 wt./wt.%
18	*n*-Hexatriacontane (C$_{36}$)	630-06-8	99%	0.9995 wt./wt.%
19	*n*-Tetracontane (C$_{40}$)	4181-95-7	97%	0.9986 wt./wt.%

| 20 | *n*-Tetracontane (C$_{44}$) | 7098-22-8 | 99% | 0.9995 wt./wt.% |
| Solvent | Carbon Disulfide | 75-15-0 | 99% | |

Table A.2 Condition of GC-FID for calibration curve.

Condition	Value
Air (kPa)	50
H$_2$ (kPa)	80
Carrier (kPa)	40
Make up (kPa)	40
Split (ml min^{-1})	30
Purge (ml min^{-1})	4

Table A.3 Retention time for each hydrocarbon component in calibration mixture.

Components	Retention time (Average)
n-Pentane (C_5)	0.25
n-Hexane (C_6)	0.45
n-Heptane (C_7)	0.87
n-Octane (C_8)	1.58
n-Nonane (C_9)	2.53
n-Decane (C_{10})	3.6
n-Undecane (C_{11})	4.69
n-Dodecane (C_{12})	5.74
n-Tetradecane (C_{14})	7.71
n-Pentadecane (C_{15})	8.61
n-Hexadecane (C_{16})	9.45
n-Heptadecane (C_{17})	10.26
n-Octadecane (C_{18})	11.02
n-Eicosane (C_{20})	12.43
n-Tetracosane (C_{24})	14.88
n-Octacosane (C_{28})	16.96
n-Dotriacontane (C_{32})	18.76
n-Hexatriacontane (C_{36})	20.32
n-Tetracontane (C_{40})	21.98

Table A.4 Density and molecular weight for component in calibration mixture. (Songphon 2011)

Component	Density (g/cm^3)	Molecular weight (g/mol)
n-Pentane (C$_5$)	0.626	72.15
n-Hexane (C$_6$)	0.659	86.18
n-Heptane (C$_7$)	0.684	100.20
n-Octane (C$_8$)	0.703	114.23
n-Nonane (C$_9$)	0.718	128.26
n-Decane (C$_{10}$)	0.730	142.28
n-Undecane (C$_{11}$)	0.740	156.31
n-Dodecane (C$_{12}$)	0749	170.33
n-Tetradecane (C$_{14}$)	0.763	198.39
n-Pentadecane (C$_{15}$)	0.769	212.42
n-Hexadecane (C$_{16}$)	0.773	226.44
n-Heptadecane (C$_{17}$)	0.777	240.47
n-Octadecane (C$_{18}$)	0.777	254.5
n-Eicosane (C$_{20}$)	0.789	282.55
n-Tetracosane (C$_{24}$)	0.797	338.66
n-Octacosane (C$_{28}$)	0.8067	394.76
n-Dotriacontane (C$_{32}$)	0.812	450.87
n-Hexatriacontane (C$_{36}$)	0.7795	506.97
n-Tetracontane (C$_{40}$)	0.7785	563.08
Carbon Disulfide	1.261	76.139

Calculation for density of calibration mixture

Density = (0.626x0.001) + (0.659x0.001) + (0.684x0.001) + (0.703x0.001) + (0.718x0.001) + (0.730x0.001) + (0.740x0.001) + (0.749x0.001) + (0.763x0.001) + (0.769x0.001) + (0.773x0.001) + (0.777x0.001) + (0.777x0.001) + (0.789x0.001) + (0.797x0.001) + (0.8067x0.001) + (0.812x0.001) + (0.7795x0.001) + (0.7785x0.001) + (0.82x0.001) + (1.261x0.001)
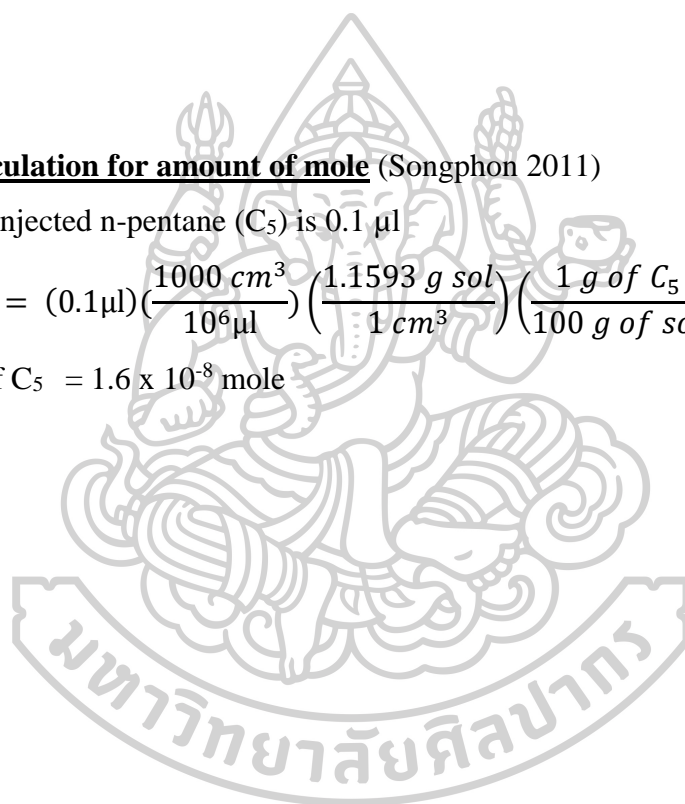
Density = 1.1593 g sol cm^{-3}

Calculation for amount of mole (Songphon 2011)
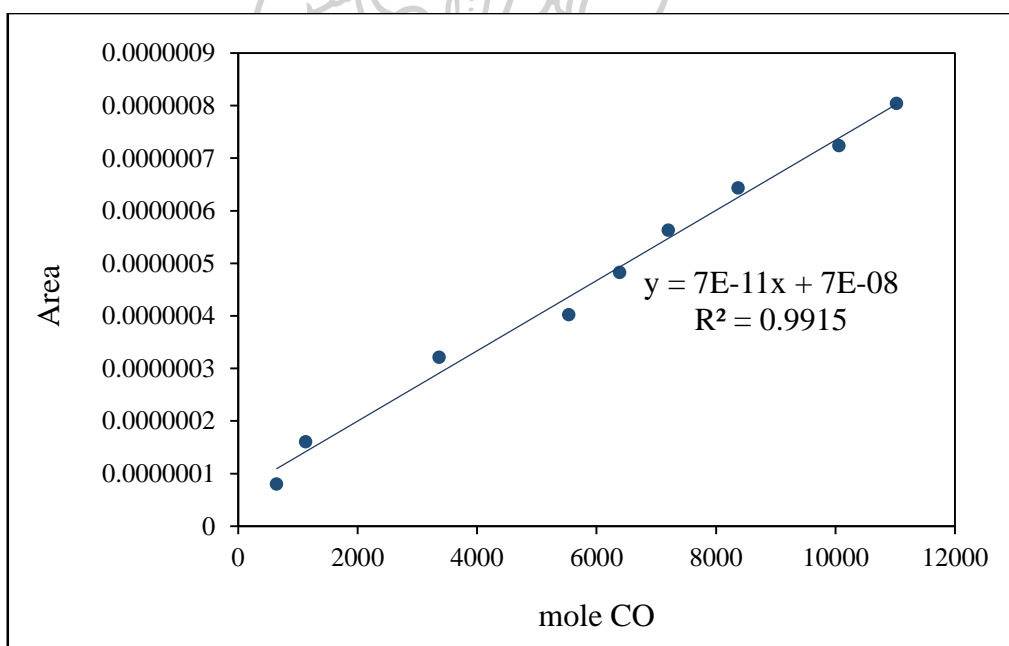
Volume of injected n-pentane (C$_5$) is 0.1 μl

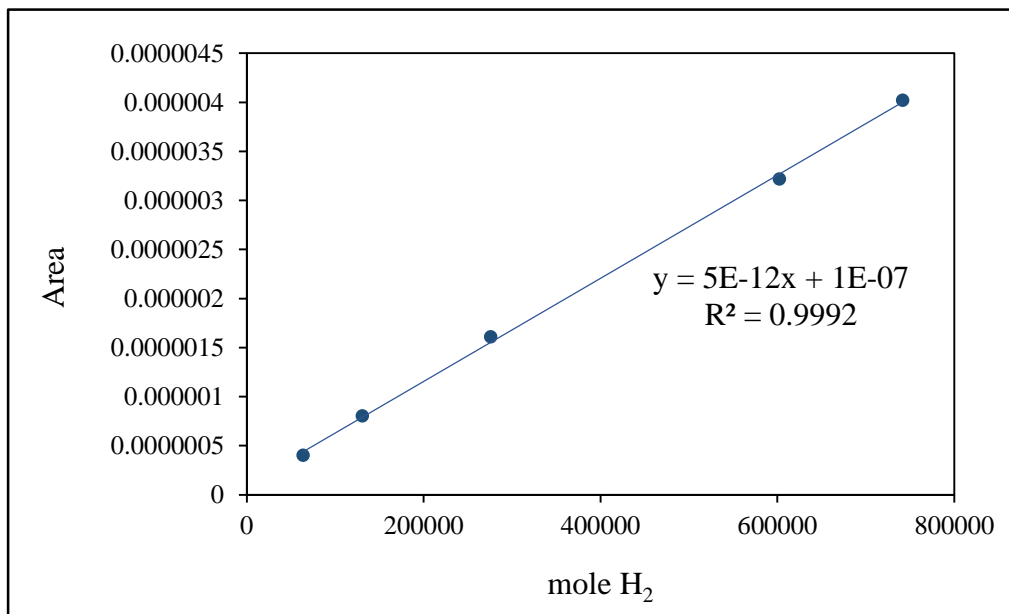Mole of C$_5$ = $(0.1 μl)(\frac{1000 \ cm^3}{10^6 μl})(\frac{1.1593 \ g \ sol}{1 \ cm^3})(\frac{1 \ g \ of \ C_5}{100 \ g \ of \ sol})(\frac{1 \ mole \ of \ C_5}{72.15 \ g \ of \ C_5})$

Mole of C$_5$ = 1.6 x 10^{-8} mole

APPENDIX B

Calibration curve for gaseous product

$y = 5E\text{-}12x + 1E\text{-}07$
$R^2 = 0.9992$

(mole H_2)

$y = 7E\text{-}11x + 7E\text{-}08$
$R^2 = 0.9915$

(mole CO)

$$y = 5E\text{-}11x + 2E\text{-}08$$
$$R^2 = 0.9986$$

mole CH_4

$$y = 7E\text{-}11x + 8E\text{-}08$$
$$R^2 = 0.9979$$

mole CO_2
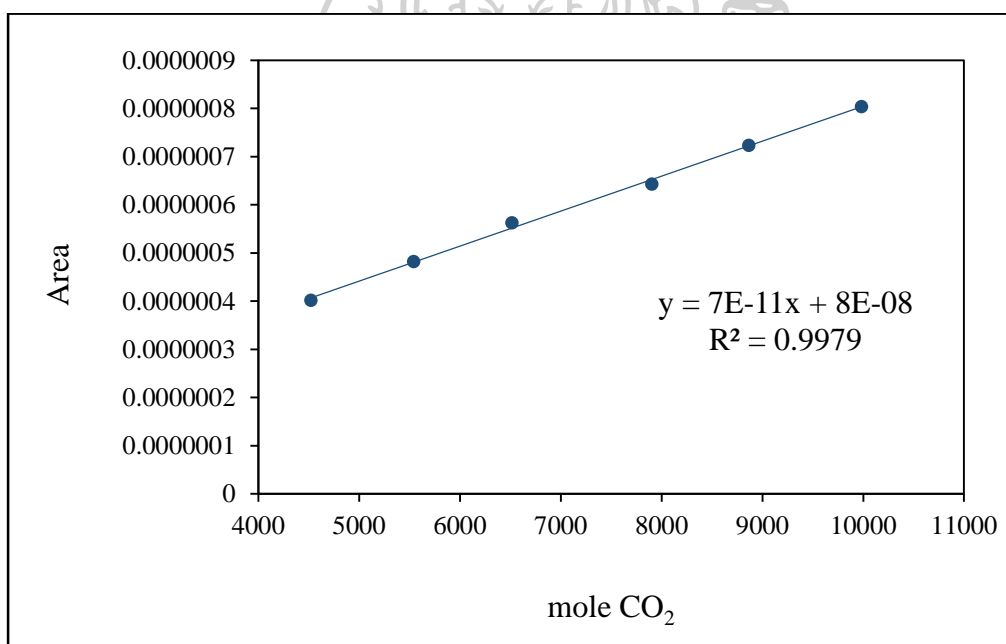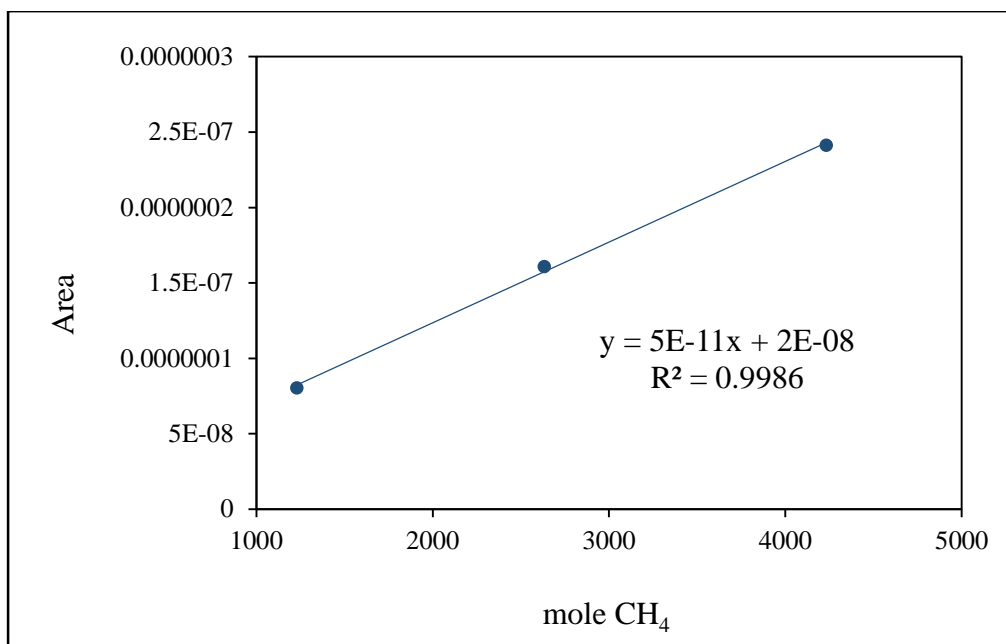
APPENDIX C

Preparation of catalysts

Table C.1 Chemicals of metal properties

Component	Molecular weight	Precursor	Molecular weight	Purity (%)
Ni	58.69	$Ni(NO_3)_2 \cdot 6H_2O$	290.81	97
Mo	95.95	$(NH_4)_6Mo_7O_{24} \cdot 4H_2O$	1235.86	81-83
Cu	63.55	$Cu(NO_3)_2 \cdot 3H_2O$	241.6	100

Table C.2 Chemicals of support properties

Component	Molecular weight	Size (mm)
$\gamma\text{-}Al_2O_3$	88.15	0.45-1.0
HZSM-5	85	0.45-1.0

<u>Calculation of NiMo/γ-Al$_2$O$_3$ catalysts by impregnation method.</u>

The sample calculation was Ni 2.45 wt.%, Mo 9.4 wt.%.

The precursor solution was calculated as follow:

Basis: 2 g of γ-Al$_2$O$_3$ support catalyst

Ni(NO$_3$)$_2$·6H$_2$O used precursor =

$$(2 \text{ g } \gamma \text{ Al}_2\text{O}_3)\left(\frac{2.45 \text{ g Ni}}{88.15 \text{ g } \gamma \text{ Al}_2\text{O}_3}\right)\left(\frac{1 \text{ mol Ni}}{58.69 \text{ g Ni}}\right)\left(\frac{1 \text{ mol Ni(NO}_3)_2\cdot6\text{H}_2\text{O}}{1 \text{ mol Ni}}\right)$$

$$\times\left(\frac{290.81 \text{ g Ni(NO}_3)_2\cdot6\text{H}_2}{1 \text{ mol Ni(NO}_3)_2\cdot6\text{H}_2\text{O}}\right)\left(\frac{1}{0.97}\right)$$

Ni(NO$_3$)$_2$·6H$_2$O used precursor = 0.284 g

(NH$_4$)$_6$Mo$_7$O$_{24}$·4H$_2$O used precursor

$$(2 \text{ g } \gamma \text{ Al}_2\text{O}_3)\left(\frac{9.4 \text{ g Mo}}{88.15 \text{ g } \gamma \text{ Al}_2\text{O}_3}\right)\left(\frac{1 \text{ mol Mo}}{95.96 \text{ g Mo}}\right)\left(\frac{1 \text{ mol (NH}_4)_6\text{Mo}_7\text{O}_{24}\cdot4\text{H}_2\text{O}}{7 \text{ mol Mo}}\right)$$

$$\times\left(\frac{1235.86 \text{ g (NH}_4)_6\text{Mo}_7\text{O}_{24}\cdot4\text{H}_2\text{O}}{1 \text{ mol (NH}_4)_6\text{Mo}_7\text{O}_{24}\cdot4\text{H}_2\text{O}}\right)\left(\frac{1}{0.82}\right)$$

(NH$_4$)$_6$Mo$_7$O$_{24}$·4H$_2$O used precursor = 0.4785 g

Calculation of NiCu/HZSM-5 catalysts by impregnation method.

The sample calculation was Ni 12.5 wt.%, Cu 2.5 wt.%.

The precursor solution was calculated as follow:

Basis: 2 g of HZSM-5 support catalyst

$Ni(NO_3)_2 \cdot 6H_2O$ used precursor =

$$(2 \text{ g HZSM-5}) \left(\frac{12.5 \text{ g Ni}}{85 \text{ g HZSM-5}} \right) \left(\frac{1 \text{ mol Ni}}{58.69 \text{ g Ni}} \right) \left(\frac{1 \text{ mol Ni(NO}_3)_2 \cdot 6H_2O}{1 \text{ mol Ni}} \right)$$

$$\times \left(\frac{290.81 \text{ g Ni(NO}_3)_2 \cdot 6H_2}{1 \text{ mol Ni(NO}_3)_2 \cdot 6H_2O} \right) \left(\frac{1}{0.97} \right)$$

$Ni(NO_3)_2 \cdot 6H_2O$ used precursor = 1.47 g

$Cu(NO_3)_2 \cdot 3H_2O$ used precursor =

$$(2 \text{ g HZSM-5}) \left(\frac{2.5 \text{ g Cu}}{85 \text{ g HZSM-5}} \right) \left(\frac{1 \text{ mol Cu}}{63.55 \text{ g Cu}} \right) \left(\frac{1 \text{ mol Cu(NO}_3)_2 \cdot 3H_2O}{1 \text{ mol Cu}} \right)$$

$$\times \left(\frac{241.6 \text{ g Cu(NO}_3)_2 \cdot 3H_2O}{1 \text{ mol Cu(NO}_3)_2 \cdot 3H_2O} \right) \left(\frac{1}{0.98} \right)$$

$Cu(NO_3)_2 \cdot 3H_2O$ used precursor = 0.22 g

APPENDIX D

Table D.1 the conversion and yield of liquid products from three operating gas.

Sample	conversion	Yield (%)	
		gasoline	diesel
30 bar of pure hydrogen			
250 v/v	97.0	1.0	70.0
500 v/v	98.89	2.7	78.6
1000 v/v	98.9	2.7	78.6
50 bar of pure hydrogen			
250 v/v	99.43	1.1	73.8
500 v/v	99.32	1.7	80.0
1000 v/v	98.89	0.9	84.6
30 bar of synthesis gas			
250 v/v	99.43	0.7	72.2
500 v/v	99.32	3.0	74.6
1000 v/v	98.89	2.7	78.6
50 bar of synthesis gas			
250 v/v	99.26	0.9	73.2
500 v/v	98.69	1.7	80.3
1000 v/v	99.81	0.8	80.3
50 bar of carbon monoxide			
500 v/v	50.14	1.0	42.5

VITA

NAME   Yuwadee Plaola

DATE OF BIRTH   4 October 1995

PLACE OF BIRTH   Ratchaburi, Thailand

INSTITUTIONS   Department of Chemical Engineering, Faculty of
ATTENDED   Engineering and Industrial Technology, Silpakorn
University

HOME ADDRESS   58/2 Donkrabuang, Photharam, Ratchaburi 70120